Available online at www.sciencedirect.com
SCIENCE DIRECT®
ELSEVIER
International Journal of Solids and Structures 43 (2006) 2959–2988
INTERNATIONAL JOURNAL OF SOLIDS and STRUCTURES
www.elsevier.com/locate/ijsolstr

On the interaction of frictional formulations with bifurcation phenomena in hyperelastic steady state rolling calculations

Ilinca Stanciulescu, Tod A. Laursen *

Department of Civil and Environmental Engineering, Duke University, Hudson Hall 121, Box 90287, Durham, NC 27708-0287, USA

Received 30 January 2005; received in revised form 16 May 2005
Available online 27 July 2005

Abstract

A finite element formulation for hyperelastic steady state rolling of inflated tires is analyzed. In particular, numerical difficulties associated with enforcing frictional conditions within such a framework are discussed. We focus in this work on adherent (i.e., no slip) friction formulations, and in addition to analyzing the numerical difficulties associated with such problems, we also study the interaction of frictional conditions with bifurcation phenomena. Such phenomena are observed in the context of multiple solutions (both stable and unstable) of the discretized system, and are also manifested in the behavior of the iterative map used to solve the nonlinear algebraic system of equations.

Keywords: Frictional formulation; Steady state rolling; Bifurcation; Iterative map; Newton–Raphson

1. Introduction

In this paper we analyze the robustness of a finite element formulation for the steady state rolling of pneumatic tires under adherent rolling conditions. Such formulations are widely utilized in the tire industry, in large part because in contrast to time-stepping techniques, the steady-state rolling approach allows the analyst to refine the mesh only in the region of the tire–road interface, without the need for a fine mesh over the entire domain and/or remeshing as a simulation proceeds (see, for example, the simple but representative meshes presented later in Figs. 4–10). A formulation commonly used for such problems is briefly presented in this introduction, while following sections are dedicated to a thorough examination of the

* Corresponding author. Tel.: +1 919 6605430; fax: +1 919 6605219.
E-mail addresses: ilinca.s@duke.edu (I. Stanciulescu), laursen@duke.edu (T.A. Laursen).

0020-7683/$ - see front matter © 2005 Elsevier Ltd. All rights reserved.
doi:10.1016/j.ijsolstr.2005.05.039

algorithmic behavior that can be observed when using such formulations. A number of interesting pathologies, associated with both the equilibrium states of the discretized system, as well as the iterative maps used to obtain these states, will be observed and to some degree analyzed. Throughout, it is important to emphasize that *all* of these pathologies are associated with the presence of frictional conditions on the tire/road interface; i.e., if one assumes frictionless response within the steady state framework, our numerical investigations have not revealed any of the difficulties that will be discussed in this paper.

In general, finite element formulations including frictional contact are subject to many numerical challenges. In the adherent rolling contact problem studied here, the numerical obstacles encountered appear to extend well beyond the norm for this difficult class of problems. Nonlinear frictional contact, as well as material and geometric nonlinearities, are among the numerical challenges associated with this problem that make existence and uniqueness of solutions difficult (if not impossible) to prove for the full range of parameters of practical interest. In fact, multiple solutions are obtained in some of the examples to be examined in this work. The occurrence of limit and bifurcation points is a common phenomenon in nonlinear structural mechanics (Kouhia and Mikkola, 1998), and such points are known to exist in particular in spinning cylinder problems even in the absence of contact conditions (Oden and Lin, 1986). When such conditions are also included into the model, contact-induced standing waves might appear (Chatterjee et al., 1999).

Building importantly upon these contributions, this paper examines for the first time the specific influence of frictional interaction upon the steady state rolling problem. We identify limit and bifurcation points of the rolling cylinder in adherent contact with a rigid surface, and examine the relationship of these points to the development of effective iterative schemes for the frictional rolling problem. We further investigate the nature of the bifurcation points that are encountered and the effect of the numerical discretization on the stability and convergence of algorithms used to compute steady state equilibria. A combination of techniques such as eigenvalue analysis and study of the bifurcations of the numerical maps are employed in order to assess the performance of the algorithm. These techniques allowed us to identify regions in the parameter space where the algorithm has a robust behavior.

1.1. Literature review

Contact problems with friction are highly nonlinear, introducing numerical difficulties in virtually any finite element formulation employed in the approximation of the solution. The nonlinearity is due not only to the material properties but also to the fact that the contact area and distribution of the contact tractions are not known beforehand. Frictional contact forces are nonconservative in the case of sliding, which also introduces nonsymmetry into a consistently linearized algorithm. Various computational aspects related to contact phenomena are discussed in Laursen (2002) and Wriggers (2002); the latter also contains an overview of rolling contact.

Examples are available in the literature on bifurcations and standing wave phenomena in the case of pure spinning cylinders and in the case of the spinning cylinders in contact with a rigid surface. Chatterjee and coworkers (see, Chatterjee et al., 1999) present an experiment in which the behavior of a rolling tire in contact with a rigid cylindrical surface is studied. The experiment described in this work identifies a critical value of the rolling speed above which a standing wave configuration is obtained.

Oden and Lin (1986) present bifurcation analyses of the free spinning cylinder and of the rotating cylinder in both frictionless and frictional contact with a flat rigid surface. The work shows that in a free spinning analysis, for small values of the angular velocity ω, the solution is unique and radially symmetric. For ω above a critical value, however, branching of the solution is encountered which manifests itself in the emergence of standing waves. The number of the peaks in the standing wave solution is exactly half of the number of elements used for discretization in the circumferential direction, which suggests that a discrete model is only able to provide a finite number of frequency components. Furthermore, these authors

show that refining the mesh will induce an increase in the number of the wave peaks without significantly changing the location of the critical point. When analyzing the case with frictionless contact, the authors observed the same behavior as in the case of pure spinning with bifurcation points that remain practically unchanged. The wavelets are almost equally distributed along the circumference and not merely concentrated in the region neighboring the contact zone.

In a later publication, Oden and Rabier (1989) developed mathematical tools that are not standard in bifurcation analysis. They studied and characterized the spectral properties of the linearized operator. The spectrum of the operator was shown to contain isolated eigenvalues, and the authors concentrated their attention on the neighborhood of every isolated eigenvalue with finite multiplicity. The conclusion of the study was that the bifurcations of the steady state solution were not due to a sudden instability of the trivial branch, and no proof was obtained to conclude whether or not this stability was lost at any point.

As mentioned earlier, one of the primary extensions of this current work beyond earlier efforts is the inclusion of friction in the analysis. In general, inclusion of Coulomb friction laws in numerical analysis presents significant numerical difficulties, the most relevant issue here being that existence and uniqueness of solutions can only be proved under special hypotheses (see for instance Han et al., 2001; Chau et al., 2002, where uniqueness results for the weak problem are established; and Han and Sofonea (2002), where in addition to such results, the continuous dependence of the solution on the data and parameters was shown). In Andersson and Klarbring (2002) a uniqueness result is established for the discretized problem, which holds only for the case of small deformations of a linear elastic body in frictional contact with a rigid obstacle. In a two-dimensional unilateral contact problem, Doudoumis et al. (1994) establish a sufficient criterion for uniqueness of the solution in the form of an upper limit for the friction coefficient.

More generally, however, such results cannot be obtained, and therefore any finite element formulation including Coulombic friction may be open to nonuniqueness. Examples of cases where solutions are not unique are widely available in the literature; to mention only a few here, we cite the results of Hassani et al. (2003, 2004) and of Ballard (1999).

1.2. Formulation of the rolling tire problem

The formulation for hyperelastic steady state rolling discussed in this paper includes most salient features for tire rolling calculations. The problem studies the rolling of an axisymmetric cylindrical body, with internal pressure and with angular velocity ω in contact with a flat rigid surface as shown in Fig. 1.

A particular case of the arbitrary Lagrangian–Eulerian representation was utilized in this study. The interested reader can find more details of the formulation in Laursen and Stanciulescu (2005), which follows from the presentation of Le Tallec and Rahier (1994). We present here only a brief overview. As is indicated in Fig. 1, we denote by $\boldsymbol{X}_0$ the undeformed, stationary configuration of the material points at some previous time, and we use $\boldsymbol{X}$ to denote coordinates in the translating (ALE) frame. We then denote by $\boldsymbol{x}$ the current position (as observed in the ALE frame), which obeys $\boldsymbol{x} = \boldsymbol{\varphi}(\boldsymbol{X}) = \boldsymbol{X} + \boldsymbol{U}(\boldsymbol{X})$, where $\boldsymbol{\varphi}(\boldsymbol{X})$ is the deformation map referred to the ALE frame, and $\boldsymbol{U}$ is likewise the displacement in this frame. For the steady state rolling case, we may then write the reference coordinates $\boldsymbol{X}$ of a material particle originally at $\boldsymbol{X}_0$ as $\boldsymbol{X} = \boldsymbol{Q}(t)\boldsymbol{X}_0$ where $\boldsymbol{Q}(t)$ is a proper orthogonal tensor representing a constant velocity rotation about some axis (in the example depicted in Fig. 1 it corresponds to a rotation about the z axis).

A variational principle for the system can be written in the usual manner as

$$0 = G_0(\boldsymbol{\varphi}_0, \overset{*}{\boldsymbol{\varphi}}_0) := \int_{\Omega_0} \rho_0 \boldsymbol{A}_0 \cdot \overset{*}{\boldsymbol{\varphi}}_0 \, \mathrm{d}\Omega + \int_{\Omega_0} [\boldsymbol{F}_0 \boldsymbol{S}_0] : [\mathrm{Grad}_0 \overset{*}{\boldsymbol{\varphi}}_0] \, \mathrm{d}\Omega - \int_{\Omega_0} \boldsymbol{f}_0 \cdot \overset{*}{\boldsymbol{\varphi}}_0 \, \mathrm{d}\Omega - \int_{\partial\Omega_0} \boldsymbol{t}_0 \cdot \overset{*}{\boldsymbol{\varphi}}_0 \, \mathrm{d}\Omega \quad (1.1)$$

which must hold for all admissible variations $\overset{*}{\boldsymbol{\varphi}}_0$. In (1.1), $\boldsymbol{A}$ denotes the material acceleration, $\boldsymbol{F}$ is the deformation gradient tensor, $\boldsymbol{S}$ is the second Piola–Kirchoff stress tensor, $\boldsymbol{f}$ is the body force vector and $\boldsymbol{t}$ is the surface traction. Subscripts 0 on all quantities indicate that they are referred to the undeformed

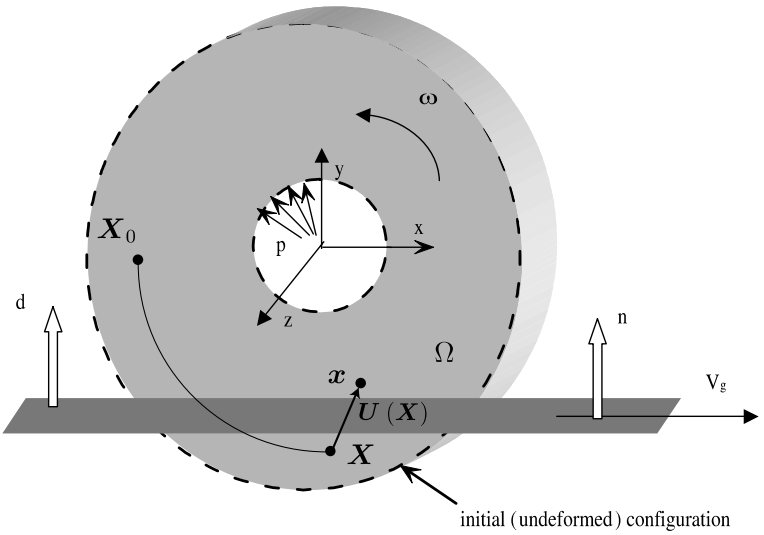

Fig. 1. Notation for the hyperelastic steady state rolling contact problem.

stationary configuration. Through a change of variables, the equations may then be expressed with respect to the ALE configuration.

Denoting the angular velocity of the rotating cylinder by ω, we follow the notation of (Le Tallec and Rahier, 1994) and define $\boldsymbol{\Pi}$ and $\boldsymbol{P}$ such that:

$$\begin{aligned} \omega\boldsymbol{\Pi} &:= \dot{\boldsymbol{Q}}\boldsymbol{Q}^{\mathrm{T}} \\ \boldsymbol{P} &:= -\boldsymbol{\Pi}^2 \end{aligned} \tag{1.2}$$

Using these notations and employing a change of variables to convert the terms from Eq. (1.1) to integrals in the ALE frame (i.e., without subscripts 0), yields the following virtual work expression (see again Le Tallec and Rahier, 1994):

$$\begin{aligned} 0 = G(\boldsymbol{\varphi}, \overset{*}{\boldsymbol{\varphi}}) := & \int_{\Omega} [\boldsymbol{FS}] : [\mathrm{Grad}\ \overset{*}{\boldsymbol{\varphi}}]\, \mathrm{d}\Omega - \int_{\Omega} \omega^2 \rho_0 [\boldsymbol{PX}] \cdot \overset{*}{\boldsymbol{\varphi}}\, \mathrm{d}\Omega - \int_{\Omega} \omega^2 \rho_0 \left(\frac{\partial \boldsymbol{U}}{\partial \boldsymbol{X}} \boldsymbol{\Pi} \boldsymbol{X} \right) \cdot \left(\frac{\partial \overset{*}{\boldsymbol{\varphi}}}{\partial \boldsymbol{X}} \boldsymbol{\Pi} \boldsymbol{X} \right) \mathrm{d}\Omega \\ & - \int_{\Omega} \boldsymbol{f} \cdot \overset{*}{\boldsymbol{\varphi}}\, \mathrm{d}\Omega - \int_{\partial\Omega} \boldsymbol{t} \cdot \overset{*}{\boldsymbol{\varphi}}\, \mathrm{d}\Omega \end{aligned} \tag{1.3}$$

which must hold for all admissible variations $\overset{*}{\boldsymbol{\varphi}}$, defined over the closure of Ω, $\bar{\Omega}$.

Material and geometric nonlinearities, pressure loaded surfaces (with spatially constant pressure p) and frictional contact between the tire and a rigid road surface are all considered in the formulation. For the tire itself, a Mooney–Rivlin hyperelastic law is used to describe the material behavior and within this context, the stored energy function considered has the form:

$$W = W^{\mathrm{vol}} + W^{\mathrm{dev}} \tag{1.4}$$

where

$$W^{\mathrm{vol}} := \frac{1}{2}\kappa(J-1)^2 \tag{1.5}$$

and

$$W^{\mathrm{dev}} = \frac{1}{2}\mu\left[(1/2+\beta)(\tilde{I}_1 - 3) + (1/2-\beta)(\tilde{I}_2 - 3)\right] \tag{1.6}$$

In (1.5) and (1.6), κ is the bulk modulus, μ is the shear modulus, β is an additional constitutive parameter, and $\tilde{I}_1$ and $\tilde{I}_2$ denote "modified" invariants of the Cauchy–Green tensor. The elements used to describe the continuum employ a $Q1$–$P0$ approximation to mitigate against potential locking phenomena associated with near-imcompressibility. The pressure loading included in our formulation follows the algorithm presented in Simo et al. (1991) and will not be explicitly discussed here.

The contact conditions imposed between the tire and ground are written in terms of two other parameters, as indicated in Fig. 1. The velocity of the ground surface relative to the moving reference frame is denoted by $\boldsymbol{v}_{\mathrm{g}}$, while contact between the ground and tire is induced by moving the rigid road surface towards the tire, with d denoting the imposed vertical motion of this surface. Although the formulation utilized allows for use of Coulomb's friction law with sliding to describe road–tire interaction, this work concentrates on the case of *adherent contact* (where $\mu \to \infty$). These contact conditions are incorporated into (1.3) by including as part of $\int_{\partial\Omega} \boldsymbol{t} \cdot \overset{*}{\boldsymbol{\varphi}}\, \mathrm{d}\Omega$ the following contact virtual work:

$$G_{\mathrm{c}}(\overset{*}{\boldsymbol{\varphi}}, \boldsymbol{\varphi}) = \int_{\partial_{\mathrm{c}}\Omega} \boldsymbol{t} \cdot \overset{*}{\boldsymbol{\varphi}}\, \mathrm{d}\Omega \tag{1.7}$$

where $\boldsymbol{t}$ are surface tractions produced by a contact constraint and $\partial_{\mathrm{c}}\Omega \subset \partial\Omega$ is taken as a subset of $\partial\Omega$ which includes that portion of the surface in contact with the ground. As in any contact problem, the geometry of the contact patch and the pressure distribution acting on it are not known a priori, which contributes substantially to the difficulty of the problem.

The contact tractions can be resolved into their normal and tangential components with respect to the ground surface, which converts (1.7) to:

$$G_{\mathrm{c}}(\overset{*}{\boldsymbol{\varphi}}, \boldsymbol{\varphi}) = \int_{\partial_{\mathrm{c}}\Omega} \boldsymbol{t}_{\mathrm{N}} \cdot \overset{*}{\boldsymbol{\varphi}}\, \mathrm{d}\Omega + \int_{\partial_{\mathrm{c}}\Omega} \boldsymbol{t}_{\mathrm{T}} \cdot \overset{*}{\boldsymbol{\varphi}}\, \mathrm{d}\Omega \tag{1.8}$$

where $\boldsymbol{t}_{\mathrm{N}}$ and $\boldsymbol{t}_{\mathrm{T}}$ represent the tractions in the normal and tangential directions. Defining the gap function as:

$$g = (\boldsymbol{\varphi}(\boldsymbol{X}) - \boldsymbol{X}_{\mathrm{r}}) \cdot \boldsymbol{n} \tag{1.9}$$

with $\boldsymbol{X}_{\mathrm{r}}$ representing an arbitrary point on the flat rigid contact surface and $\boldsymbol{n}$ denoting the unit normal to the rigid surface, the Kuhn–Tucker conditions describing the normal part of the contact interaction may be stated as:

$$g(\boldsymbol{X}) \geqslant 0 \tag{1.10}$$

$$\boldsymbol{t}_{\mathrm{N}}(\boldsymbol{X}) \cdot \boldsymbol{n} \leqslant 0 \tag{1.11}$$

$$(\boldsymbol{t}_{\mathrm{N}}(\boldsymbol{X}) \cdot \boldsymbol{n}) g(\boldsymbol{X}) = 0 \tag{1.12}$$

for all $\boldsymbol{X} \in \partial_{\mathrm{c}}\Omega$. Implementation of these conditions can be readily accomplished using either penalty or augmented Lagrangian approaches; the interested reader may consult Laursen (2002) for more details. In this work, we present results corresponding primarily to penalty treatments, although both alternatives have been implemented and tested.

An adherent contact model in the tangential direction may be incorporated by appending to the Kuhn–Tucker conditions an additional condition on the tangential sliding velocity $\boldsymbol{v}_{\mathrm{T}}$ (to be further defined below):

$$\|\boldsymbol{v}_{\mathrm{T}}\| = 0 \tag{1.13}$$

which is also to be satisfied for all $\boldsymbol{X} \in \partial_{\mathrm{c}}\Omega$. From an implementation standpoint, this condition is enforced via a penalty method, where the tangential traction is defined to be a penalization of the tangential velocity, as is discussed briefly below.

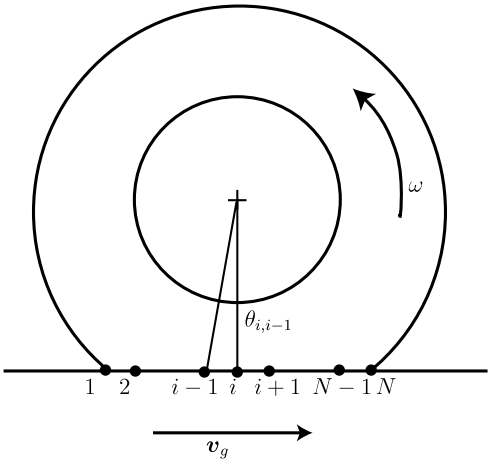

Fig. 2. Node numbering convention for approximation of contact velocities.

1.2.1. Relative velocity measure

The relative velocity of a point $\boldsymbol{X} \in \partial_c\Omega$ with respect to the roadway can be computed as a consequence of the steady state kinematic assumptions (see, Laursen and Stanciulescu, 2005), and may be expressed in terms of the relative road velocity $\boldsymbol{v}_g$ as:

$$\boldsymbol{v}^{\text{rel}} = \boldsymbol{V} - \boldsymbol{v}_g = \boldsymbol{F}[\boldsymbol{\omega} \times \boldsymbol{X}] - \boldsymbol{v}_g \tag{1.14}$$

From the standpoint of implementation, there are many conceivable ways of approximating $\boldsymbol{v}^{\text{rel}}$. Here, this relative velocity is numerically approximated by using a backward difference scheme along circumferential rings of nodes in contact (the numbering is represented in Fig. 2), and the numerical approximation to the tangential relative velocity at a node i can be expressed (see, Laursen and Stanciulescu, 2005) as:

$$\boldsymbol{v}_{\text{T}_i} \approx [\boldsymbol{I} - \boldsymbol{n} \otimes \boldsymbol{n}]\boldsymbol{v}^{\text{rel}}(\boldsymbol{X}_i) = [\boldsymbol{I} - \boldsymbol{n} \otimes \boldsymbol{n}]\left\{\frac{\omega}{\theta_{i,i-1}}(\boldsymbol{x}_i - \boldsymbol{x}_{i-1}) - \boldsymbol{v}_g\right\}. \tag{1.15}$$

It is important to note that this approximation is only valid for structured meshes containing rows of nodes aligned in the circumferential direction about the tire; in the event that such a nodal arrangement does not exist, an alternative approximation must be utilized.

1.2.2. Algorithmic treatment of adherent contact conditions

We consider here a penalty regularization of the frictional problem, introducing a tangential penalty ϵ_{T} which can be different from the normal penalty ϵ_{N}. In discretized form, the virtual work can be summarized as:

$$\sum_{\text{Mooney–Rivlin elements } e} G^e(\overset{*}{\boldsymbol{\varphi}}, \boldsymbol{\varphi}) - \sum_{\text{pressure faces } e} G_p^e(\overset{*}{\boldsymbol{\varphi}}, \boldsymbol{\varphi}) + \sum_{i=1}^{N} A_i \frac{g_i}{\epsilon_{\text{N}}} \delta g_i = \sum_{i=1}^{N} A_i \boldsymbol{t}_{\text{T}_i} \cdot \delta \boldsymbol{x}_i \tag{1.16}$$

where the frictional traction $\boldsymbol{t}_{\text{T}_i}$ is evaluated *at all* $i = 1, \ldots, N$ on the contact patch (and for all circumferential parallels of nodes) such that it satisfies Eqs. (1.10)–(1.13). The A_i represent the surface Jacobians (tributary areas) associated with each contacting node. For the adherent contact conditions, the tangential stress would be computed as:

$$\boldsymbol{t}_{\text{T}} = -\frac{\boldsymbol{v}_{\text{T}}}{\epsilon_{\text{T}}} \tag{1.17}$$

It may be readily verified that the velocity measure utilized here, as well as the corresponding friction law, satisfy the principle of frame indifference.

1.3. Overview of this study

The formulation we have briefly summarized performs well for most problems to which it is applied, and indeed, variants of this approach appear to be in rather widespread use in industry. However, upon closer examination, it is not difficult to find instances where a Newton–Raphson algorithm is unsuccessful in converging to an equilibrium configuration. Such convergence failures do not occur due to ill conditioning (except sometimes in the vicinity of critical points), nor are they usually characterized by explosively divergent sequences of iterations. Rather, such failures are often manifested through convergence to periodic solutions instead of fixed points, and quite often, the failure to converge would not even be noticed except when strict convergence tolerances (on the order of machine precision) are utilized. Furthermore, in loading sequences where convergence is successfully achieved, the existence of multiple solutions has been verified in several cases. These observations suggest that bifurcation phenomena are strongly connected with this problem, and this paper explores the interaction of such bifurcation phenomena with the frictional formulation and with the performance of the classical Newton–Raphson iterative scheme.

Accordingly, Section 2 introduces the methods of analysis (both of critical points, and of iterative maps) that are used in our analysis. With these tools in hand, Section 3 is fully dedicated to numerical simulations of the steady state rolling problem. We present examples of multiple equilibria, along with a study of the spectral signature of the stiffness matrix. Examples presenting the algorithmic behavior of the Newton–Raphson scheme are also included and the similarities and differences between the configurations belonging to the same periodic solution are analyzed. We end our study by presenting numerical examples in which the regions of robust behavior of the algorithm as well as the problematic regions are identified.

2. Analysis techniques for critical points and bifurcation phenomena associated with iterative maps

In this section we briefly review some of the techniques to be used in characterizing the bifurcation behavior of the steady state rolling problem.

2.1. Critical points: Methods of identification and characterization

Any finite element formulation can be expressed in the general schematic form:

$$\boldsymbol{R}(\boldsymbol{x},\boldsymbol{\lambda}) = \boldsymbol{0}; \quad \boldsymbol{R} : \mathbb{R}^{n+k} \to \mathbb{R}^{n} \tag{2.1}$$

where $\boldsymbol{R}$ may be thought of as the residual (here, an out of balance force), $\boldsymbol{x}$ is the vector of unknowns, nodal displacements in our case (the dimension n is the number of degrees of freedom in the system) and $\boldsymbol{\lambda}$ is the vector of generalized loading parameters (with dimension k).

For nonlinear problems, the system of Eq. (2.1) may be solved with the classical Newton–Raphson method, where the "load" (i.e. $\boldsymbol{\lambda}$) is often applied incrementally. However, the standard incremental approach may behave poorly (lose quadratic convergence or even diverge) in the vicinity of critical points. Therefore it is of high interest to be able to identify these critical points and also to determine their nature (limit points, bifurcation points). Convergence problems usually appear at or after these values, and stabilizing methods and/or different algorithms may be necessary to overcome them.

The Newton–Raphson method involves the linearization of the system (2.1). The consistent tangent $D_x\boldsymbol{R}$ is defined by its elements, K_{ij}:

$$K_{ij} = \frac{\partial R_i}{\partial x_j} \tag{2.2}$$

and the algorithm will advance the solution from iteration p to iteration $p+1$:

$$\boldsymbol{x}^{p+1} = \boldsymbol{x}^p - \left(D_x \boldsymbol{R}(\boldsymbol{x}^p)\right)^{-1} \boldsymbol{R}(\boldsymbol{x}^p) \tag{2.3}$$

The sequence $(\boldsymbol{x}^p)_{p=1}^{\infty}$ is the discrete Newton–Raphson trajectory of the initial iterate $\boldsymbol{x}_0$. If this sequence is convergent, i.e. $\exists \lim_{p\to\infty} \boldsymbol{x}^p$, then the iterative algorithm was successful in obtaining a solution, and the initial iterate $\boldsymbol{x}_0$ was in the basin of attraction of this solution.

An equilibrium configuration $(\boldsymbol{x}, \boldsymbol{\lambda})$ is a *regular point* of the solution path if $\det \boldsymbol{K}|_{(\boldsymbol{x},\boldsymbol{\lambda})} \neq 0$; otherwise, it is called a *singular/critical/stability point*. A schematic representation of these different stability cases is presented in Fig. 3. Critical points can either be *limit points* or *bifurcation points*. Schematized representations of these cases are shown in Fig. 3(b) and (c).

Limit points are configurations on the solution path where the Jacobian is singular and the vector $\frac{\partial \mathbf{R}}{\partial \lambda}$ does not belong to the space spanned by the column vectors of the Jacobian. Limit points are characterized by the fact that equilibrium configurations do not exist in their neighborhood for values of the load greater that the critical value (Riks, 1972). This is not usually true for bifurcation points. In the neighborhood of a bifurcation point, a system can have more than one possible equilibrium configuration with different stability properties. There are several types of bifurcations: asymmetric, stable symmetric, and unstable symmetric. These can occur at limit or turning points, or they can be multiple limit point bifurcations.

There are two classes of methods one can utilize to compute the critical points. An *indirect method* indicates a critical point with the help of a detecting parameter that is monitored while tracing the equilibrium path in an incremental manner. For instance, the parameter can be chosen to be either the determinant of the tangent stiffness matrix or its smallest eigenvalue. In a *direct method*, the critical point is included as an unknown in the system of equations, thus leading to an extended system with additional unknowns whose solution will directly give the location and nature of the point. For instance, Wriggers and coworkers (see, Wriggers et al., 1988; Wriggers and Simo, 1990) considered the eigenvector equation $\boldsymbol{K}\boldsymbol{\psi} = 0$ as the stability point condition, while in Planinc and Saje (1999) a method that uses the determinant of the stiffness matrix is presented.

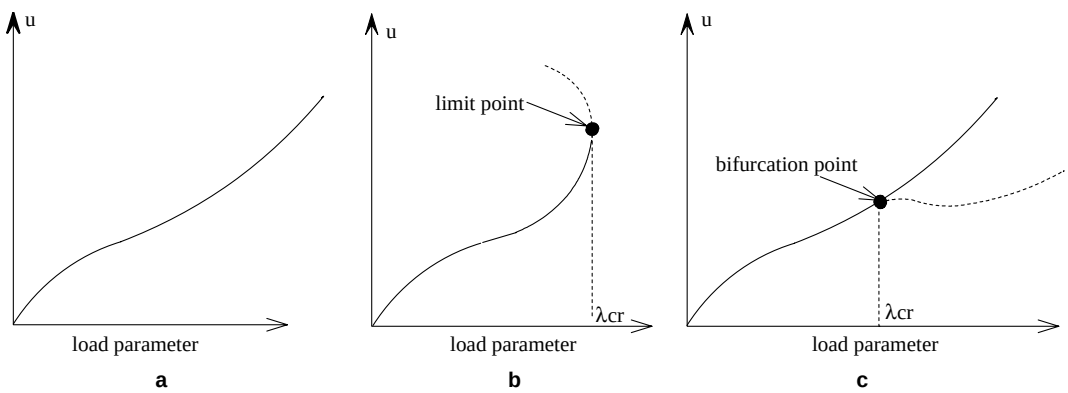

Fig. 3. Stability cases—schematic representation for a 1-DOF system. (a) Monotonically increasing all equilibrium configurations are regular points. (b) One singular point (limit point) on an equilibrium path. (c) Bifurcataion point. Equilibrium path splits, more than one configuration exists for $\lambda > \lambda_{cr}$.

2.2. Eigenvalue analysis

The method we use here to locate the critical points is an indirect one. Using an incremental approach, we start from an unloaded configuration and gradually apply the load to our structure while monitoring the eigenvalue signature of the stiffness matrix along the equilibrium path.

The equilibrium path is unique and stable (see Fig. 3a) as long as we have a positive definite Jacobian, $\det \boldsymbol{K} > 0$. When a critical state is encountered, it may be identified by the value of the controlled parameter for which the determinant becomes null for the first time (or when the smallest real eigenvalue becomes negative). Since an incremental approach can only accurately obtain the critical point with a refinement of the incremental procedure, standard methods will only return approximate values, since any eigenvalue analysis is also very sensitive to perturbations when the matrix is nearly singular.

Once a point on an equilibrium path is obtained, one can also examine the stability of an equilibrium configuration. This is a local property and concerns the behavior of the equilibrium path in the neighborhood of that configuration. For a conservative (self-adjoint) system, the equilibrium is stable if the matrix is positive definite, neutrally stable if the matrix is positive semidefinite and unstable if the matrix is not definite. For a *nonsymmetric system* of the type analyzed here, the eigenvalues might be complex valued (pairs of complex conjugate eigenvalues since the matrix is real), and along with bifurcations corresponding to singularities of the stiffness matrix, other types of critical states (associated with the presence in the spectrum of $\boldsymbol{K}$ of purely imaginary eigenvalues) can be identified. These states are mathematically characterized as local Hopf bifurcations (Hale and Kocak, 1991). For a nonconservative loading, the system's loss of stability might manifest itself not only by the system evolving towards a different equilibrium state but also by the system presenting an unbounded motion. This is manifested numerically as a *divergence* situation.

2.3. Bifurcations in iterative maps: Convergence analysis of the Newton–Raphson algorithm

The nonlinear system of equations given in (2.1) can also be written as $\boldsymbol{F}^{\text{int}}(\boldsymbol{x}, \boldsymbol{\lambda}) = \boldsymbol{F}^{\text{ext}}(\boldsymbol{\lambda})$ (note that $\boldsymbol{R} = \boldsymbol{F}^{\text{ext}} - \boldsymbol{F}^{\text{int}}$), thus moving to the right hand side the terms that do not depend on $\boldsymbol{x}$. Solutions are sought using a Newton–Raphson iterative scheme. At each iteration the linearized system, $\boldsymbol{K}(\boldsymbol{x}^i) \cdot \Delta \boldsymbol{x} = \boldsymbol{R}^i$ is solved and the unknowns are updated in the usual manner via $\boldsymbol{x}^{i+1} = \boldsymbol{x}^i + \Delta \boldsymbol{x}$ (or with line search, which may be also utilized). For the linearized system to be a consistent Newton–Raphson iteration, we require:

$$\boldsymbol{K}^i = \boldsymbol{K}(\boldsymbol{x}^i) = \left(\frac{\partial \boldsymbol{F}^{\text{int}}}{\partial \boldsymbol{x}} \right) \Bigg|_{\boldsymbol{x}=\boldsymbol{x}^i} \tag{2.4}$$

If the Jacobian is not singular, the function $\boldsymbol{g}$ defining the Newton–Raphson iterative map may be identified from the previous equalities as:

$$\boldsymbol{g}(\boldsymbol{x}^i) = \boldsymbol{x}^i + (\boldsymbol{K}^i)^{-1}(\boldsymbol{F}^{\text{ext}} - \boldsymbol{F}^{\text{int}}(\boldsymbol{x}^i)) \tag{2.5}$$

Some definitions regarding elements and characteristics of an iterative map (Hale and Kocak, 1991) that might be useful are listed in Appendix A.

A successful Newton–Raphson sequence of iterations will converge toward a fixed point $\bar{\boldsymbol{x}}$, i.e.

$$\lim_{i \to \infty} \boldsymbol{g}^i(\boldsymbol{x}^0) = \bar{\boldsymbol{x}}$$

and if this convergent sequence exists, $\bar{\boldsymbol{x}}$ is called an *asymptotically stable fixed point* of the map, with the initial iterate thus belonging to the basin of attraction of the stable fixed point. Convergence to a fixed point represents the simplest possible algorithmic behavior of the map, but nonfixed periodic or dense (and asymptotic to periodic) orbits are also typical for maps. In the case of the Newton–Raphson map they are of great interest since they imply a failure of the root finding method.

3. Numerical examples

The formulation discussed in this paper was implemented in FEAP, a finite element program developed by Prof. Taylor (2003) at The University of California at Berkeley.

All convergence results are quoted in terms of a relative "energy norm" criterion, which in the context of a Newton–Raphson iteration scheme is defined as:

$$\text{Relative energy norm} = \frac{\boldsymbol{R}^i \cdot \Delta \boldsymbol{d}^i}{\boldsymbol{R}^0 \cdot \Delta \boldsymbol{d}^0} \tag{3.1}$$

In this expression, $\boldsymbol{d}^i$ refers to the search direction calculated at Newton–Raphson iteration level i, $\boldsymbol{R}^i$ refers to the residual (or right hand side) which produces this search direction, and the superscripts 0 in the denominator denote the respective quantities in the first Newton–Raphson iteration in a load step.

3.1. Example problems for this study

In the sequel, two example problems will be used to demonstrate the performance of the frictional rolling formulation. In the first of these, a small rubber disk of outer radius 200 mm and inner radius 66 mm was used as a simplified idealization for a tire (see Figs. 4–7, which will subsequently be referred to as simple disk models 1–4). As can be seen from the figures, these meshes allow us the opportunity to investigate the effect of mesh refinement in the footprint region. Starting with the "basic" mesh, numbered 1, with ten nodes (equally spaced) in contact on each parallel, 2 elements along the radius and two elements wide, the mesh was refined by proportionally increasing the number of elements up to mesh number 4 (which has 40 nodes along one parallel of the contact patch, 8 elements along the radius and 8 elements across its width). The problem is solved using an angular velocity of $\omega = 48.7$ rad/s, a rolling velocity of $v_g = 10170$ mm/s, and Mooney–Rivlin material properties $\beta = 0.4219$, $\mu = 12.0106$, density $\rho = 0.104 \times 10^{-9}$ daN s^2/mm^4 and $\kappa = 100$ daN/mm^2. Penalties of $\epsilon_N = \epsilon_T = 10^{-8}$ were used in simulation of this problem, with adherent contact assumed and an internal pressure set to $p = 0.03$ daN/mm^2.

The second problem studied, representing a highly idealized truck tire, is depicted in Fig. 8, with the left and right portions of the figure presenting again varying degrees of refinement of this problem. In this

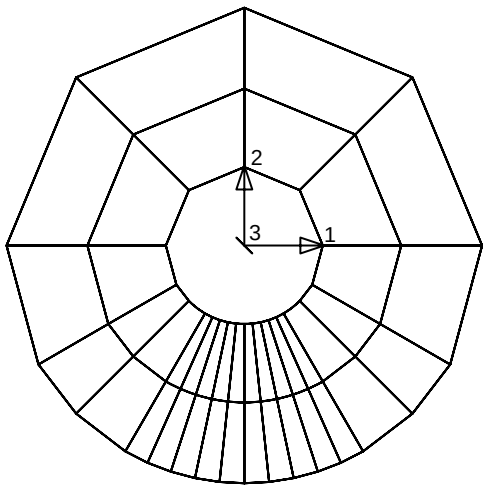

Fig. 4. Simple disk; model 1.

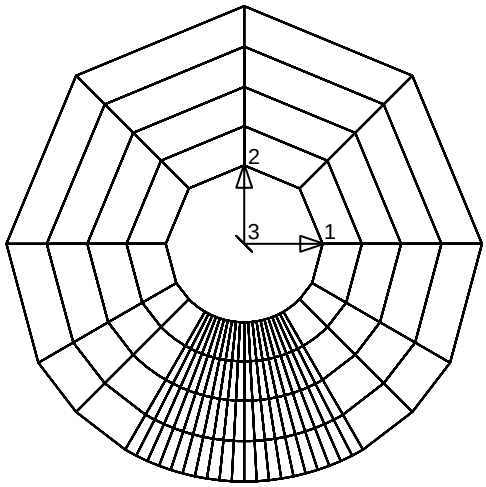

Fig. 5. Simple disk; model 2.

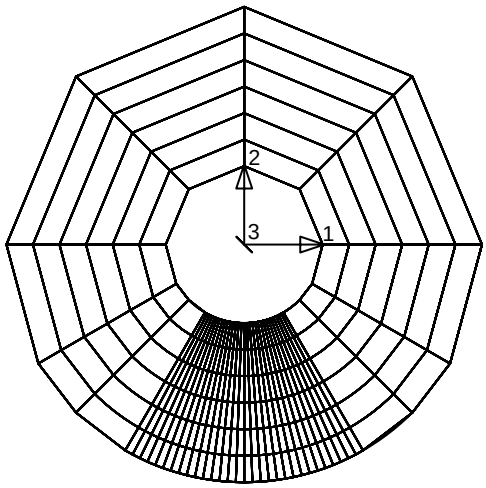

Fig. 6. Simple disk; model 3.

simulation, the material properties for the Mooney–Rivlin material are as follows: $\beta = -0.39473$, $\mu = 0.73$, $\kappa = 100$ daN/mm^2. The density is $\rho = 0.104 \times 10^{-9}$ g/mm^3, the angular velocity $\omega = 48.7$ rad/s and the ground velocity is prescribed to be $v_g = -9999$ mm/s. The penalties for both the tangential and the normal constraint in this problem are taken as $\epsilon_N = \epsilon_T = 10^{-7}$ and the internal pressure is $p = 0.03$ daN/mm^2.

An example result obtained for the simple disk problem is presented in Figs. 9 and 10 for the most refined mesh (model 4) with $d = 20$ mm. In many cases such as this, the algorithm presented provides a reliable and stable solution. However, for some combinations of road displacement d, ground velocity v_g, and angular velocity ω, we encountered Newton–Raphson iterative sequences that were unable to reach the solution and settled into a cycle, periodically visiting a finite set of configurations. Multiple converged solutions were obtained for some combinations of parameters. All these difficulties are analyzed in the following sections.

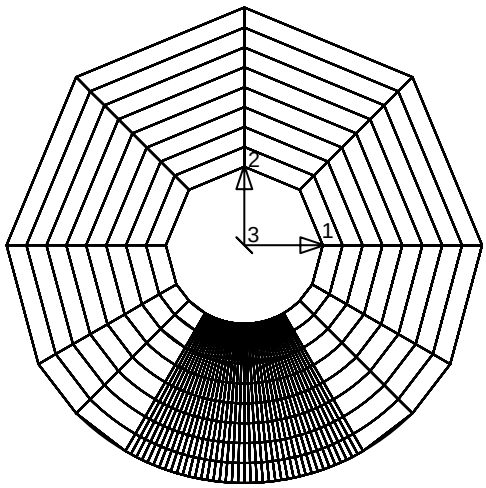

Fig. 7. Simple disk; model 4.

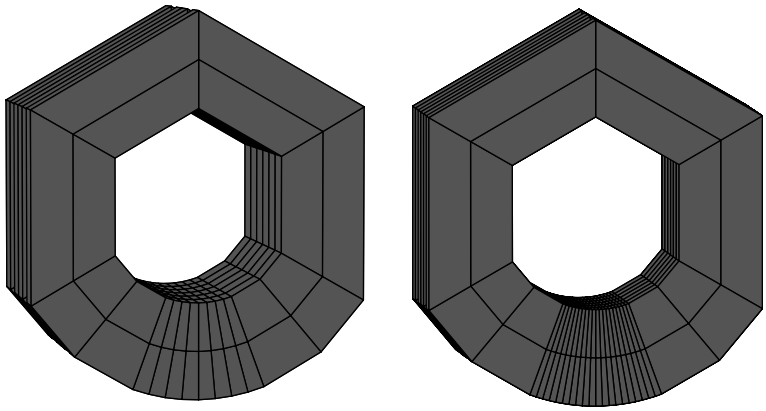

Fig. 8. Idealized truck tire test problem. Discretizations with (a) 16 and (b) 28 meridians.

As a preview of the types of difficulties encountered, we present in Figs. 11 and 12 the total reactions on the contact patch for model 4 of the simple disk problem, in the case where a loading sequence of 300 load steps of $\Delta d = 0.1$ mm is imposed. For some displacements along this sequence, convergence was not reached. This behavior is discussed in Section 3.3. As seen in Fig. 11, the normal reaction exhibits a smooth monotonic increase with the increase in displacement. However, the tangential component appears to be discontinuous with plateaus and jumps (as shown in Fig. 12). Each jump separates states having a different contact patch geometry (i.e. a different set of nodes in contact). Moreover, the plot of the tangential component brings up another unusual behavior manifested in the form of "negative" jumps. If the shape of the contact patch is examined before and after such a jump, we can see that there are actually nodes appearing to go out of contact at that point (even though the roadway has been forced farther up into the tire). This is usually not observed in contact problems when loading is applied in a monotonic incremental manner. A possible explanation for such behavior is given in Section 3.4.

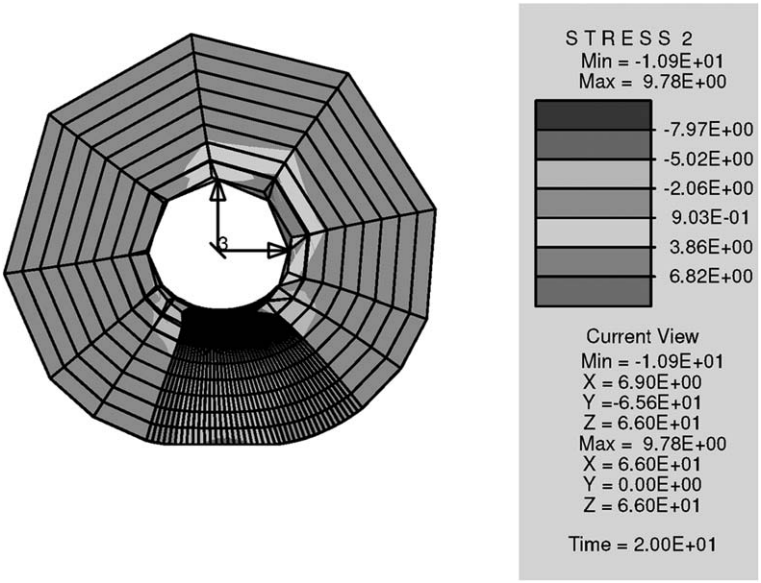

Fig. 9. Contour plot of the 2–2 stress [daN/mm^2], simple disk, model 4.

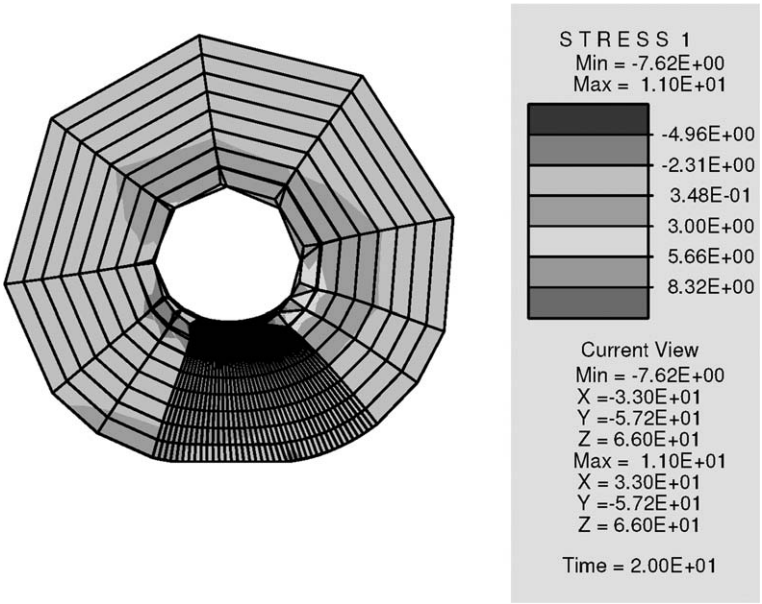

Fig. 10. Contour plot of the 1–1 stress [daN/mm^2], simple disk, model 4.

The idealized truck tire problem, using the coarser mesh depicted in the left of Fig. 8, allows us another opportunity to examine the pathologies occasionally encountered with this formulation of the problem—in this case, multiple equilibria. Many analyses were performed with different incremental loading paths, and two of them resulted into two different solutions corresponding to the same loading level. Results in the form of the contour plots of the tractions on the contact patch are presented in Figs. 13 and 14. In the first

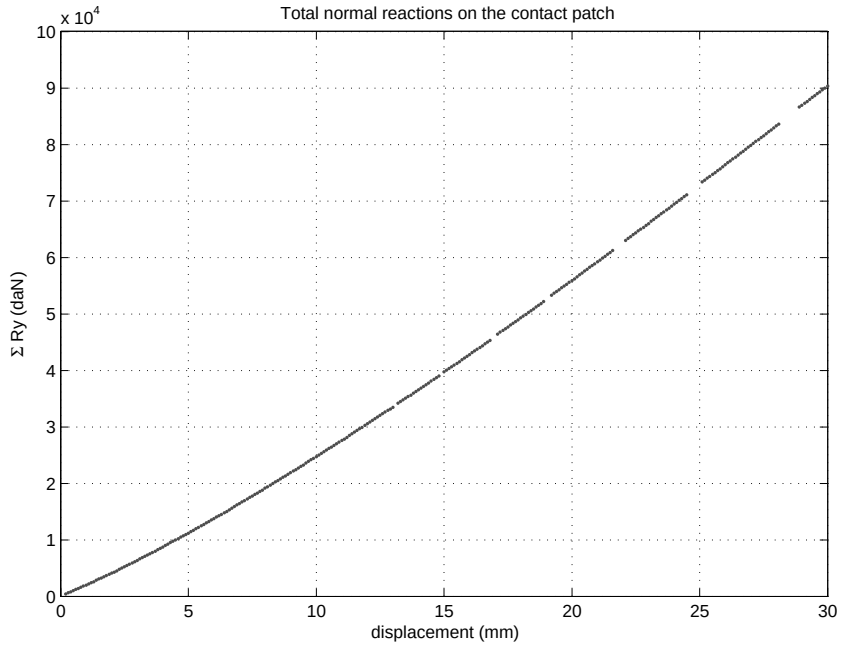

Fig. 11. Total normal reaction on contact patch; simple disk model 4.

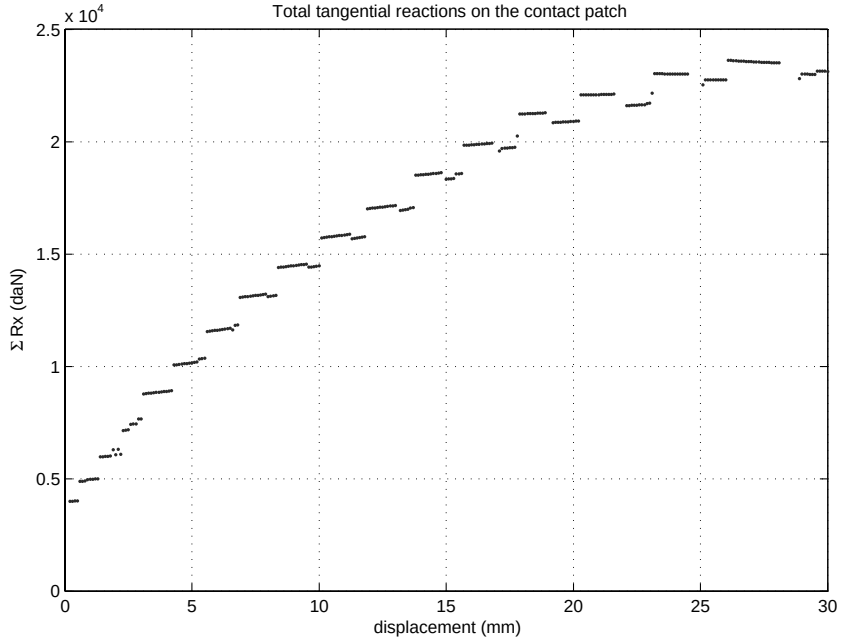

Fig. 12. Total tangential reaction on contact patch; simple disk model 4.

case (plots at the top), the total load was applied in 10 equal steps and in the other, the same load was applied in one step.

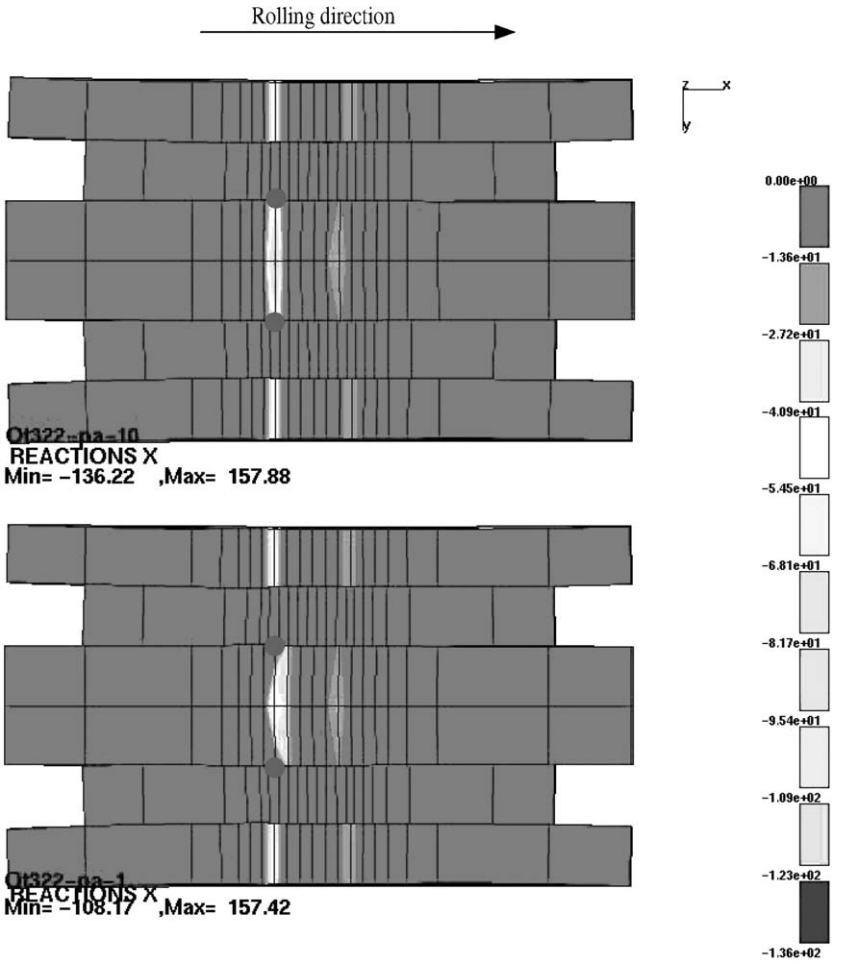

Fig. 13. Horizontal tractions corresponding to multiple equilibria for idealized truck tire.

The two solutions are very close to each other. The difference comes only from the two nodes that are clearly identified on the images. The solution depicted in the top images is an equilibrium configuration with those two nodes in contact, while the other one has the two nodes out of contact.

3.2. Eigenvalue analysis results

Since the multiple solutions observed above suggest the occurrence of bifurcation points along the loading path, the method presented in Section 2.2 was employed to identify the bifurcation points on the loading path suggested by the presence of these multiple solutions. The method relies on monitoring the spectral signature of the stiffness matrix at equilibrium positions along the loading path.

We will present and discuss results obtained for the idealized truck tire depicted in Fig. 8; subsequently, we will refer to the mesh on the left as test problem M16, and the more refined mesh on the right as M28. In these two problems, as well as others we have studied, the progression of the eigenvalue signature with increasing road displacement d tended to follow a similar pattern. For loading levels corresponding to small

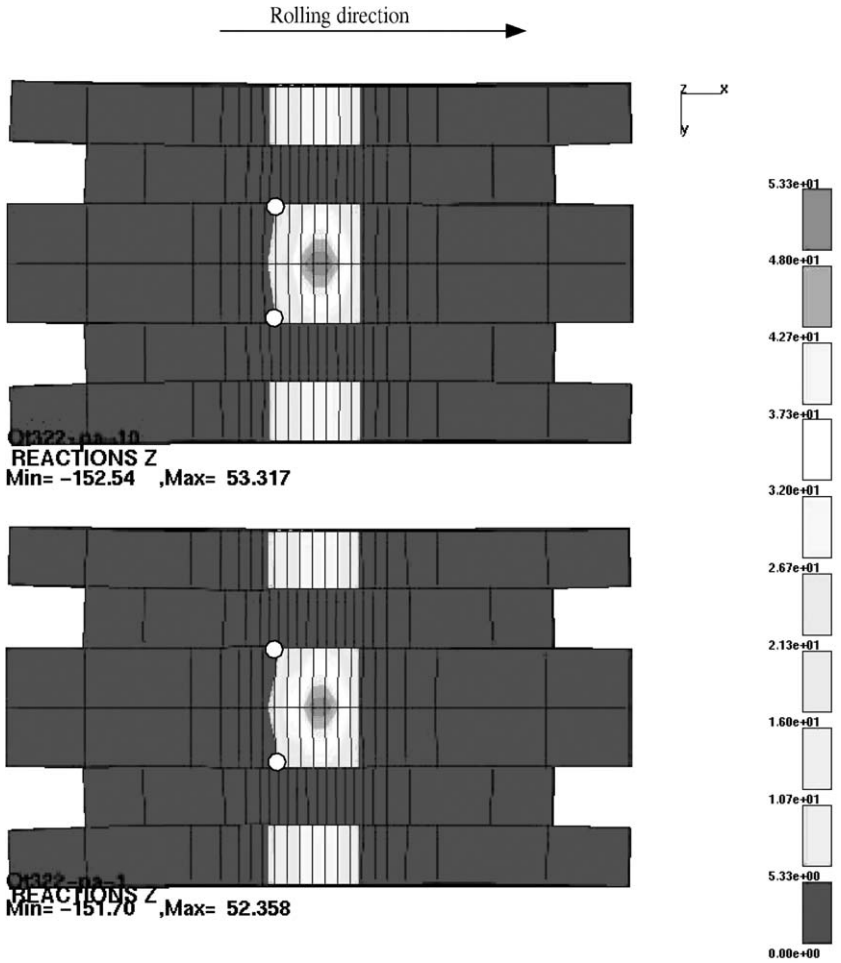

Fig. 14. Vertical tractions corresponding to multiple equilibria for idealized truck tire.

values of the road displacement d, the spectrum contains only eigenvalues with positive real components and null or insignificant imaginary components. This is precisely what one would expect, as for small loads the system is very nearly a self-adjoint system. For intermediate values of d, one obtains a spectral signature with a concentration of eigenvalues on or close to the real axis, accompanied in this case with a set of eigenvalues that all have approximately the same real part and large imaginary parts (see Fig. 15 for a result typical of models M16 and M28). The occurrence and general location of these imaginary eigenvalues does not seem to depend strongly on the size of the elements for this and the other problems studied.

At some value of the displacement (denoted subsequently as the *critical displacement*) the eigenvalues start crossing the complex axis and eigenvalues with negative real parts appear in the spectrum. The value of the critical displacement displays a strong dependence on the discretization, and decreases when refining the mesh. For refined meshes, several critical points tend to be concentrated in a small interval; in this interval, the stiffness matrix is obviously ill conditioned and therefore converged solutions are hard to obtain.

In models M16 and M28, the refined model M28 presented critical points earlier than did M16. In both cases, the first critical point appeared in the form of a singular stiffness matrix with a single real eigenvalue crossing the 0 threshold. Above this value of the road displacement, the spectral signature in the right half

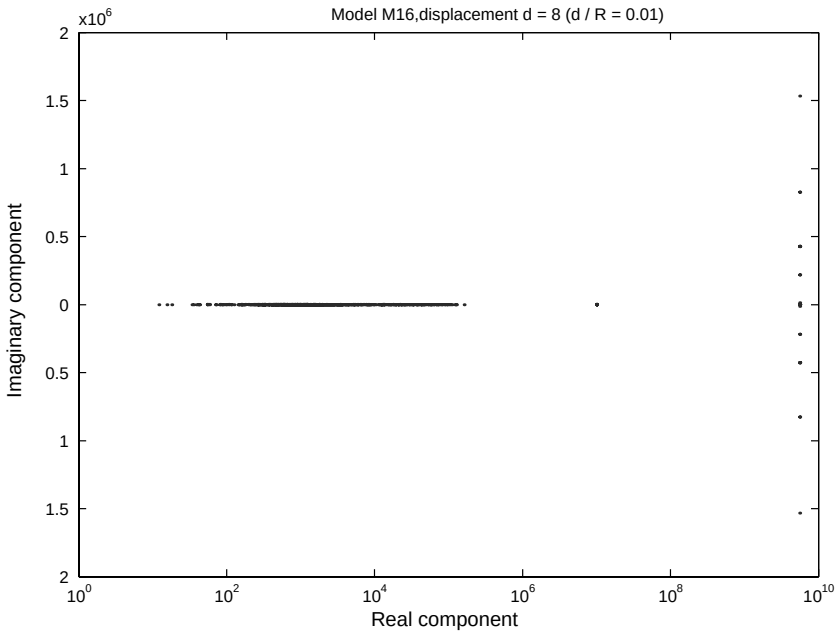

Fig. 15. Typical spectral signature for models M16 and M28 at an intermediate road displacement, before the critical point is reached.

of the complex domain remained similar to signatures prior to the critical point as presented in Fig. 15. Fig. 16 displays a post-critical spectral image for model M28, with the top portion of the figure depicting the half of the complex plane with positive part, and the bottom portion depicting a zoom of those eigenvalues which have crossed over the imaginary axis. This behavior confirms the presence of Hopf points. The multiple equilibria presented for this problem in Section 3.1 correspond to a value of the road displacement above the first Hopf point.

3.3. Bifurcation of the iterative map k-cycles

As mentioned earlier, for many of the problems studied using this formulation, we were unable to obtain convergence in a given step, but obtained instead a stable periodic cycle under the iterative map. None of the states visited under the map satisfy a machine precision convergence tolerance, but in fact, the energies associated with many of these unsuccessful iterations are quite small. Furthermore, in such situations, the iterations never diverge, the displacements remain bounded and the Newton–Raphson iterations settle into a stable k-cycle.

We present below results from such a case, encountered when analyzing the simple disk in an adherent calculation using the most refined mesh (model 4) with a ground velocity $v_g = 10\,000$ mm/s in the x-direction. In this example, the cycle has a periodicity of 2, the map iterates indefinitely between two distinct configurations, visiting one of them at every other iteration as shown in Fig. 17. This is most likely a situation where the two configurations are not in the basin of attraction of any stable branches of the solution of the discretized problem (if such a stable solution even exists). The condition number of the stiffness matrix is normal for both configurations (i.e. similar to condition numbers obtained for converged solutions around this level of deformations). This behavior is very different from what is encountered when ill conditioning or singularity of the stiffness matrix are contributory factors (in the vicinity of critical points, for instance).

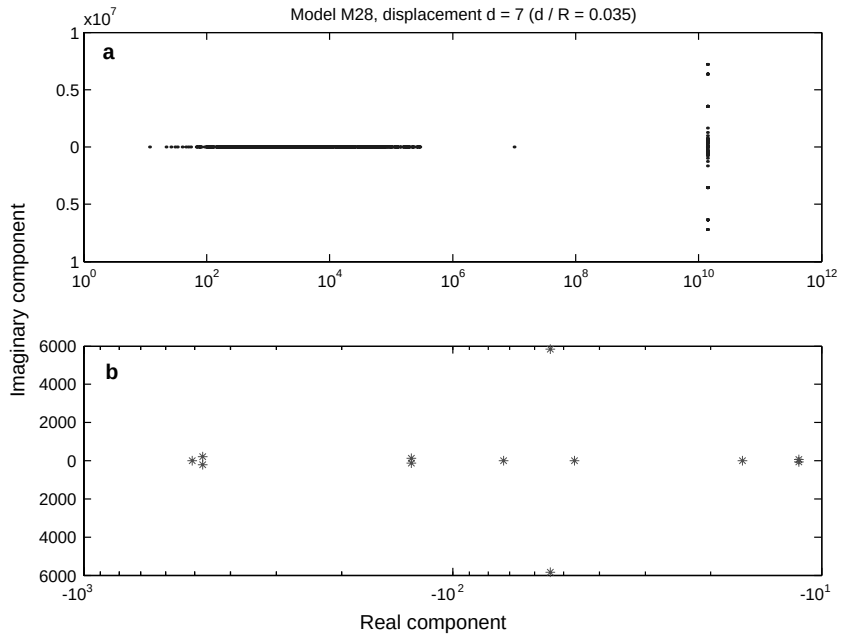

Fig. 16. Spectral signature for model M28 at a road displacement above the value of the first Hopf point. (a) Right half of complex plane (i.e., eigenvalues with positive real part); (b) zoom on eigenvalues with negative real part.

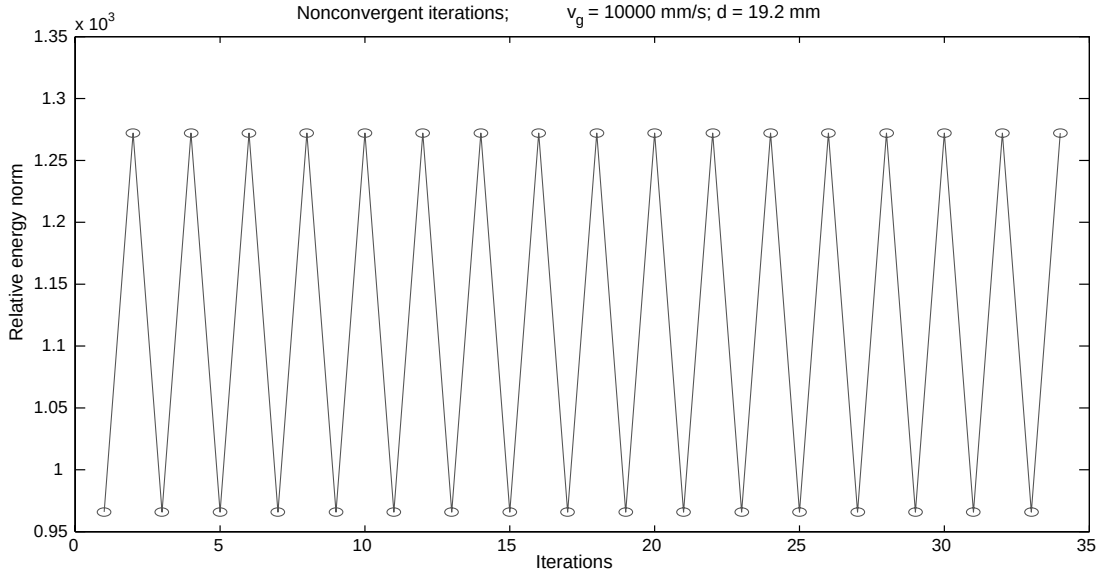

Fig. 17. Energy norm levels for a stable 2-cycle obtained during Newton–Raphson iterations at $d = 19.2$ mm, for the simple disk problem with model 4.

In examining the traction fields corresponding to the two states, one can observe no significant differences as far as the normal components are concerned. The only noticeable difference appears in the tangen-

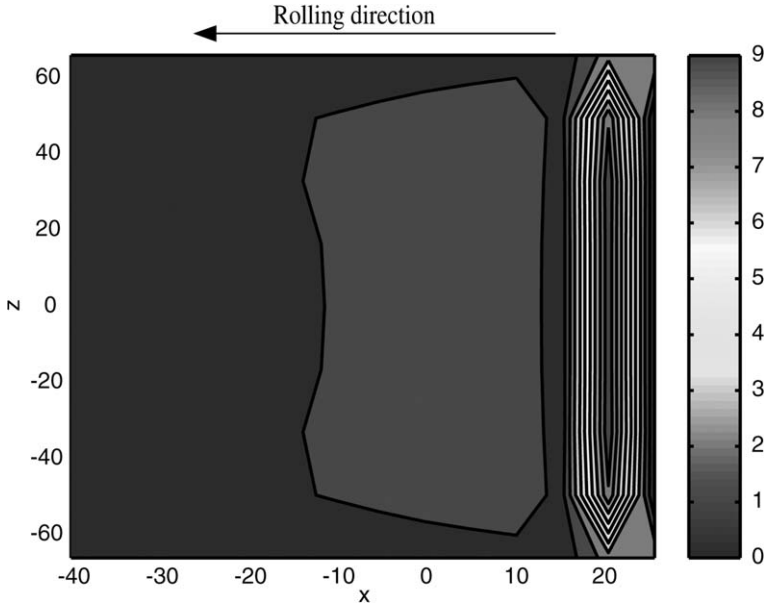

Fig. 18. Contour plot of tangential tractions (daN/mm^2) for the first 2-periodic point corresponding to Newton–Raphson iterations at $d = 19.2$ mm; simple disk problem, model 4.

tial fields (see the contour plot of tangential tractions presented in Figs. 18 and 19). The two configurations differ only slightly, the discrepancy coming from one of them having two more nodes in contact more than the other. It this case, these are the two leading nodes on the most lateral parallels. Similar situations can be observed in some other cases with trailing nodes oscillating in and out of contact during the iterations. In some sense, it is the same qualitative difference that was observed in the case of the multiple solutions.

This behavior is not unique to this problem and parameter set, and k-cycles appeared often in our study. The example presented here involves the occurrence of a 2 cycle, however k-cycles (with $k = 3, 4, 5$) were also obtained in some other cases for adherent contact. k-cycles with larger k's seem to be characteristic for larger load values and occur more often on the coarser meshes than on the refined ones. We also encountered situations where for a given d on a particular loading sequence, a stable k-cycle appeared, while a different loading sequence produced a period one solution (equilibrium) at the same load level. From these observations we can conclude that the behavior of the iterative map is qualitatively dependent on the range of the road displacement, thus proving the existence of the *bifurcations of the iterative map*.

To better describe this dependency, we looked at the outcome of the Newton–Raphson iterations for $d \in [0, 30]$ mm applied in in a number of different road displacement increments Δd in the model 4 problem. These results may be seen in Fig. 20, where the different configurations of non converged steps are represented by their relative energy norm and in the abscissa we have the variation of the parameter d. For small values of d, a stable fixed point (''period one'' solution) is obtained which represents the equilibrium configuration (note that since only nonconverged states are shown, regions with a stable fixed point are indicated by no data points being present at the d in question). As d is increased, the solution bifurcates (by either disappearing or becoming unstable), and a stable periodic solution takes its place or coexists with it. In some other cases, non periodic and probably dense stable orbits may appear. We can also observe that a period one solution recovers its stability along certain intervals of the parameter d. In this application, the first period k solution with $k \neq 1$ was identified at $d = 8.8$ mm. It is also worthy of note that the

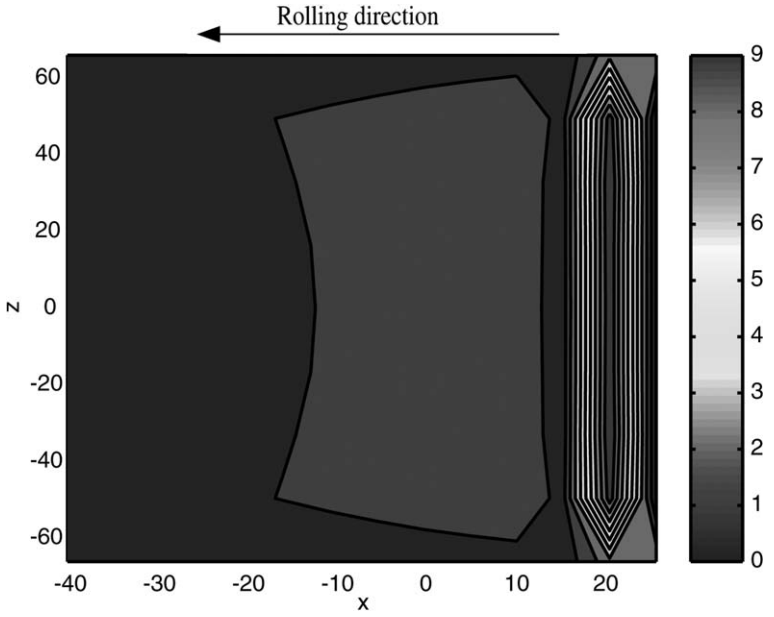

Fig. 19. Contour plot of tangential tractions (daN/mm^2) for the second 2-periodic point corresponding to Newton–Raphson iterations at $d = 19.2$ mm; simple disk problem, model 4.

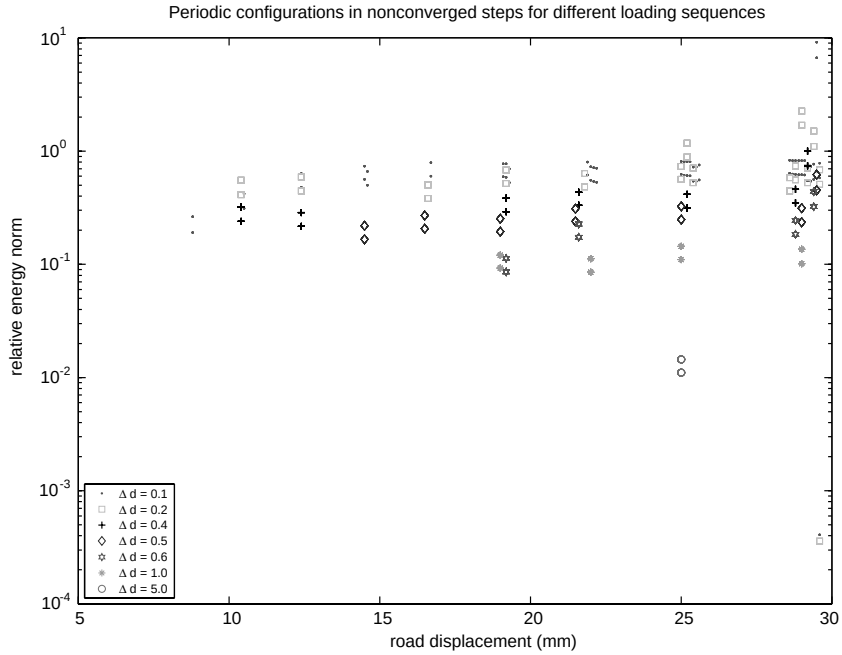

Fig. 20. Nonconverged configurations along the loading path obtained from the Newton–Raphson iterative map and the energies associated with them: simple disk problem, model 4.

road displacements at which the k-cycles occur tend to be the same for a variety of road displacement increments.

Similar analysis on less refined meshes guided us to a very interesting observation. Large relative energy norms (sometimes on the order of 10^4) that appeared for some configurations in the periodic cycles, never led to a divergence situation and the periodic periodic solution obtained under the map kept its stability.

Finally, periodic orbits have been shown to exist in some other similar applications presented in the literature. For example, in Narayanan and Sekar (1996), the case of two cylinders (one rigid, one flexible) in rolling contact is analyzed. Presence of stable and unstable periods 2–4 solutions coexisting with stable or unstable period one (fixed point) solution was proven for some ranges of the bifurcation parameter.

3.4. Bifurcation of the solution of the discretized problem

As we have seen, the frictional rolling problem exhibits bifurcations in the Newton–Raphson map used to locate equilibrium states, and when convergence is obtained, one may often identify multiple solutions for the same discretized problem. To further investigate the solution bifurcations which can occur along an equilibrium path, we present a test performed on model 4 for the simple disk, using a ground velocity of 10 170 mm/s. The total loading of $d = 30$ mm was applied in four different loading sequences (300 steps $\times$ 0.1, 60 steps $\times$ 0.5, 30 steps $\times$ 1 and 15 steps $\times$ 2); all sequences contained some steps whose solutions under the map were stable k-cycles. The plots given in Figs. 21 and 22 present the total reactions on the contact patch corresponding to displacements $d = 2i$ mm with $i = 1, \ldots, 15$.

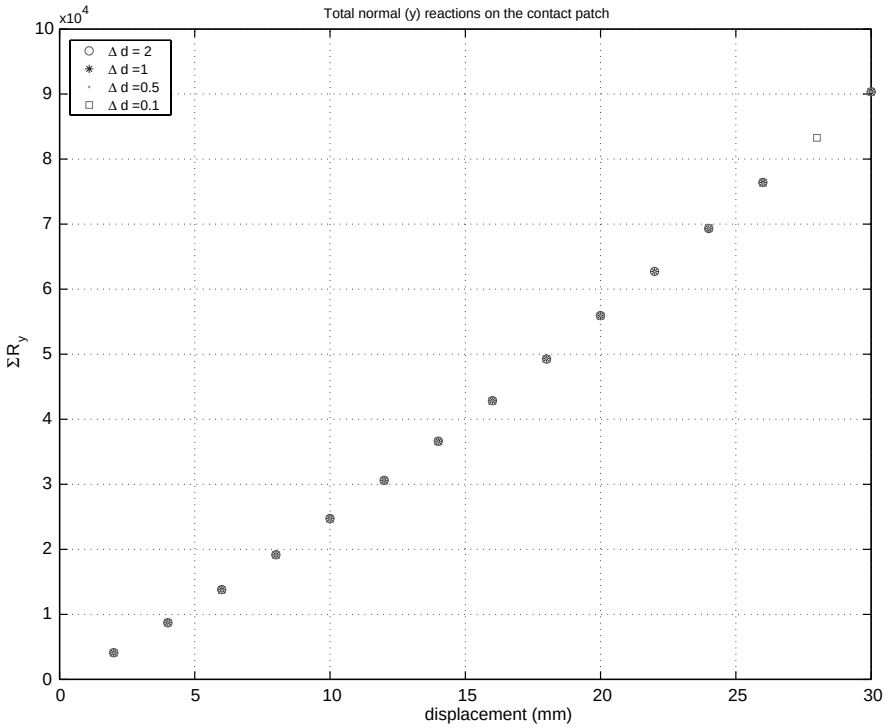

Fig. 21. Total normal reaction on the contact patch, simple disk problem, model 4. For steps where convergence was not obtained, no data point is shown.

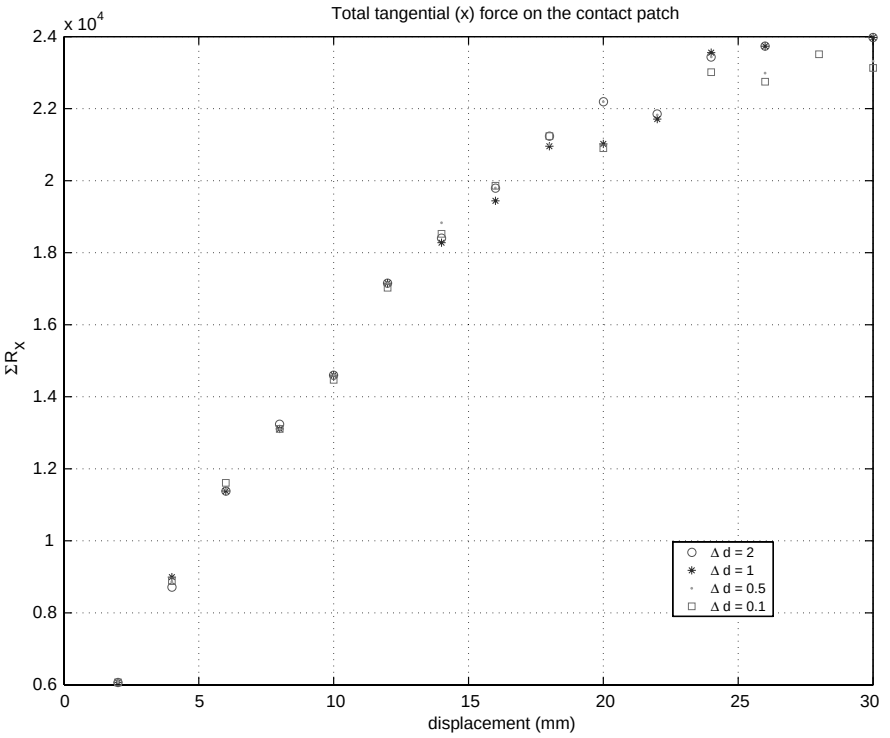

Fig. 22. Total tangential reaction on the contact patch, simple disk problem, model 4. For steps where convergence was not obtained, no data point is shown.

Depending on the loading sequence, for equivalent road displacement we obtained two or more solutions each having a different set of nodes in contact. Solutions are in general close to each other, and if we examine the reactions on the contact surface, the differences in the normal components are insignificant (see Fig. 21), the only noticeable difference appearing in the tangential component (shown in Fig. 22). It is this component that is the most sensitive to the discretization. This difference is quite small and comes from the difference in size of the contact area, whose boundary is slightly shifted. In this particular case, the largest difference that can be observed was between two solutions obtained at $d = 20$ mm, one along the loading sequence with $\Delta d = 2$ mm and one with $\Delta d = 0.1$ mm. The shapes of the contact patches obtained for these two cases are presented in Figs. 23 and 24. We will denote by "solution 1" the solution at $d = 20$ mm obtained during a loading sequence with $\Delta d = 2$ mm and by "solution 2" the solution at $d = 20$ mm obtained during a loading sequence with $\Delta d = 0.1$ mm. The contour plot of the the tangential tractions corresponding to these solutions are presented in Figs. 25 and 26.

We may now recall the case introduced in Section 3.1 with nodes appearing to go out of contact along an incremental monotonic loading path. Having proved that multiple numerical solutions associated with a given discretized problem exist, we can now suggest a justification for what first appeared to be inexplicable. If multiple numerical solutions exist, these negative jumps may be manifestations of the numerical solution jumping between different branches. To ensure that the algorithm stays on one branch along the whole loading sequence, we probably have to run the problem with a small displacement increment for each load step. This is particularly challenging since the different minima seem to be close to each other so the load step has to be indeed very small (in our experiences, often impractically so).

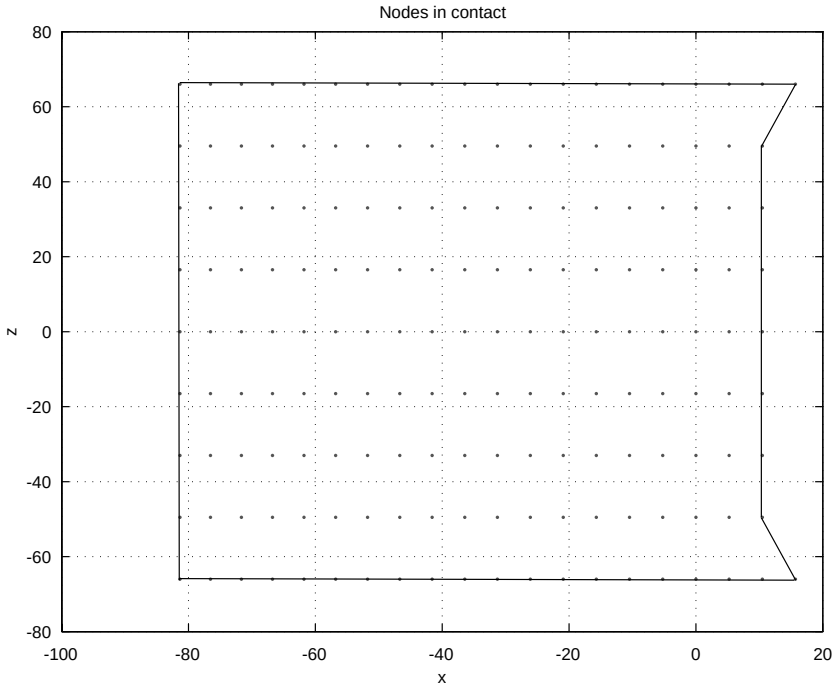

Fig. 23. Shape of the contact patch for solution 1, simple disk problem, model 4.

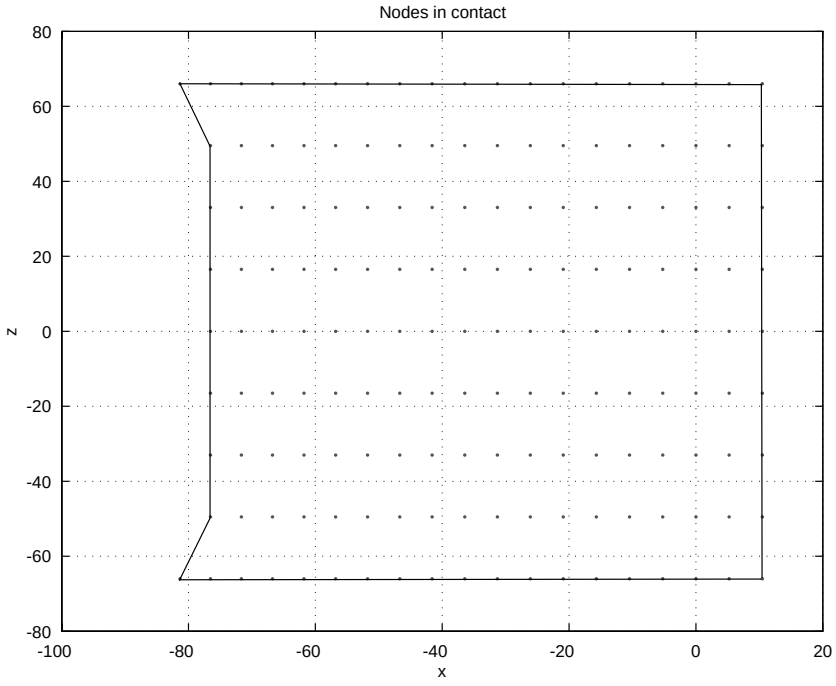

Fig. 24. Shape of the contact patch for solution 2, simple disk problem, model 4.

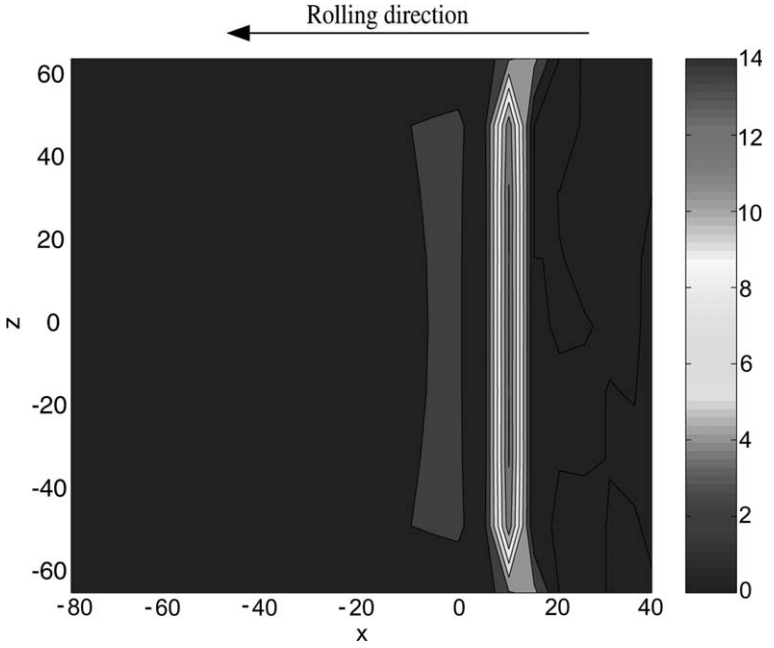

Fig. 25. Contour plot of the tangential tractions for solution 1, simple disk, model 4.

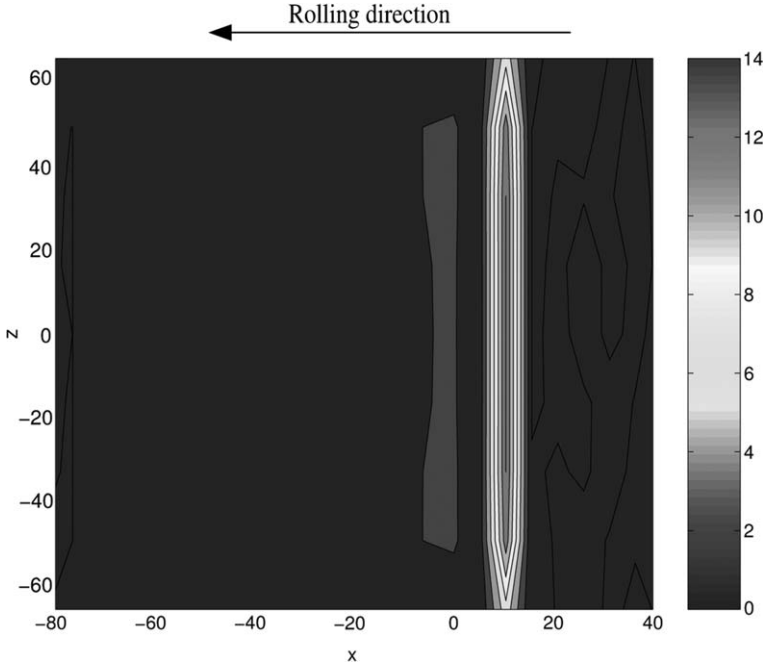

Fig. 26. Contour plot of the tangential tractions for solution 2, simple disk, model 4.

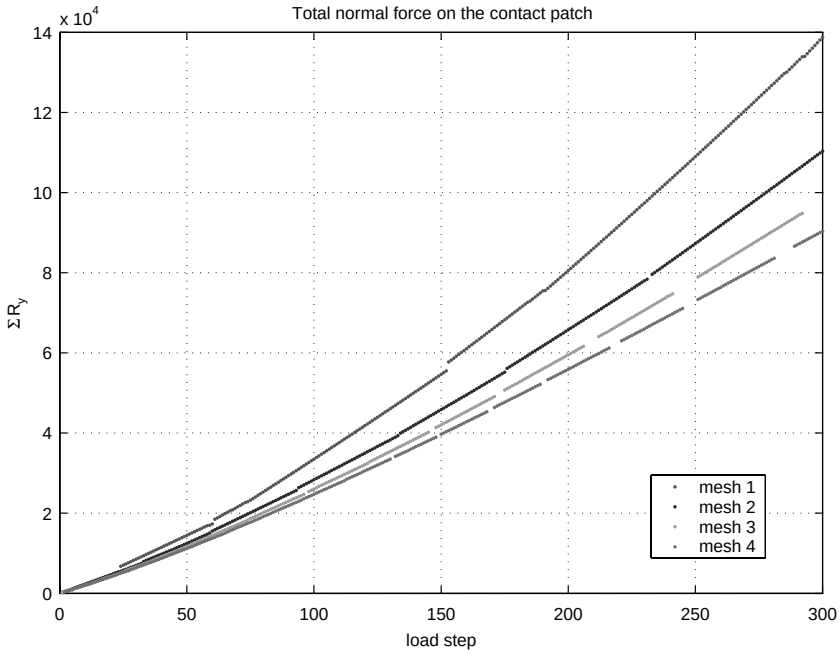

Fig. 27. Total normal reactions obtained during simulations of 4 simple disk model problems. At values of d where a solution is not shown for a loading sequence, convergence was not obtained.

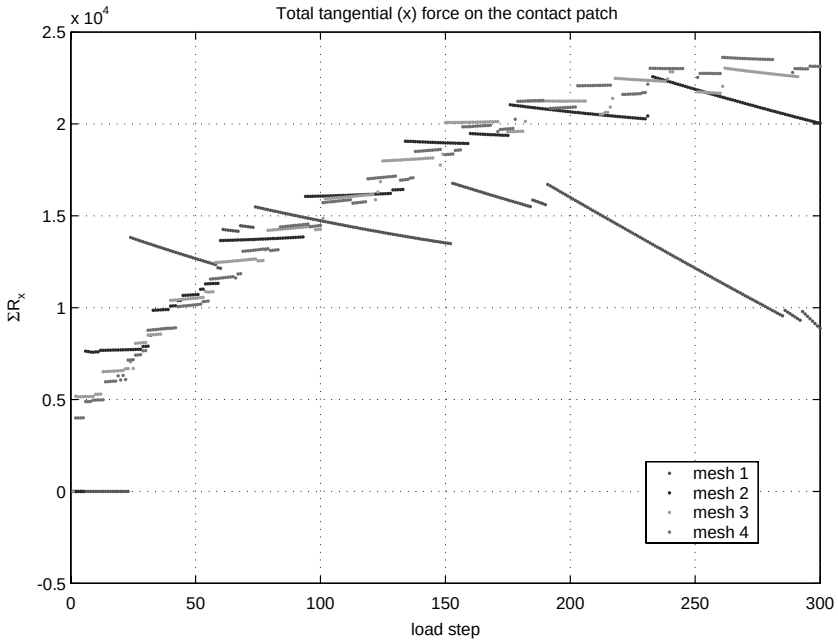

Fig. 28. Total tangential reactions obtained during simulations of 4 simple disk model problems. At values of d where a solution is not shown for a loading sequence, convergence was not obtained.

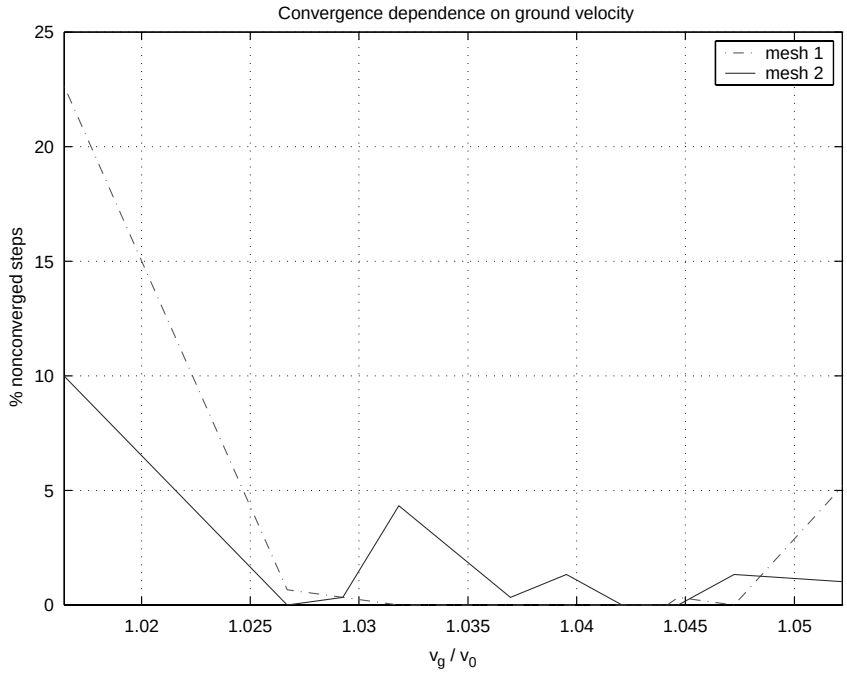

Fig. 29. Influence of the ground velocity on the algorithmic behavior.

3.5. Mesh refinement study

For a ground velocity of $v_g = 10\,170$ mm/s the evolution of the normal and tangential reaction along the loading path are presented in Figs. 27 and 28 for four simple disk models introduced in Section 3.3 (see Figs. 4–7).

While a monotonic variation in the normal reaction can be observed as the mesh is refined, the tangential reactions exhibit the discontinuities emanating from the frictional formulation, and do not display a clear monotonic variation when refining the discretization. However, in both the normal and tangential components, we can observe that the difference between two consecutive refinements decreases with the refinement.

3.6. Influence of the ground velocity

As might be expected, the ground velocity v_g has a strong influence on the algorithm's ability to converge to an equilibrium solution. This is intuitively reasonable, since under the assumed condition of steady state rolling the angular velocity ω and the ground velocity v_g should not be entirely independent, but related through the rolling radius of the tire under steady state conditions (which of course, is also unknown). One might expect, therefore, that inauspicious choices for v_g may not even be physically consistent with the steady state assumption. Accordingly, we study here the influence of the ground velocity on the ability of the algorithm to recover solutions during loading paths characterized by the same incremental road displacement Δd. For the simple disk problem considered previously, a plot of the percentage of nonconvergent load steps (for models 1 and 2) as a function of the ground velocity is presented in Fig. 29. The initial count of nonconverged steps was done on an incremental sequence employing 300 load steps of $\Delta d = 0.1$ mm.

The coarsest mesh (model 1) presents a quite large interval of the ground velocity ($v_g \in [10\,050, 10\,200]$ mm/s) for which convergence was obtained easily. The representation in the plot was normalized and has v_g/v_0 in the abscissa, where we denoted by v_0 the velocity of a point on the outer circumference of the cylinder assumed to be rigid, $v_0 = \omega R = 9740$ mm/s. Refining the mesh is seen to have an unwanted effect on the algorithmic behavior, as a higher percentage of nonconverged steps along a loading sequence are observed in those cases. However, a "good interval" for v_g can still be observed on the plot for model 2. In both problems, most of the nonconverged steps correspond to loading levels for which converged solutions can be obtained either via another loading sequence or simply by applying the full displacement in one step.

As might be expected, there are values of the ground velocity for which a steady state solution is unlikely to exist; as stated above, it makes no sense to look for such a solution in regimes of strong acceleration or braking. Indeed, when the ground velocity is either increased or decreased significantly, reaching a period one solution is more and more unlikely. Even the coarser meshes display a large number of nonconverged states in this instance. Eventually, the numerical behavior will evolve towards divergence situations when very large or small values of v_g are used.

4. Conclusions

Since the finite element formulation used in this study presupposes a steady state rolling condition, it is of no surprise that indeed there is a specific range of the ground velocity for which this algorithm will have a robust behavior. Numerical difficulties have been seen to affect the algorithmic behavior once we try to solve for a steady state solution in ranges of the rolling velocity that correspond to braking or accelerating. An interesting fact associated with this observation is that the occurrence of periodic stable solutions associated with the nonlinear iterative Newton–Raphson map have been observed. These often coexist with period one solutions which seem to have limited basins of attraction, therefore requiring a good initial iterate in order to be recovered by the root finding method.

Moreover, *multiple numerical solutions* have been shown to exist. The local minima for these solutions are close to each other, thus making difficult to follow one of the solutions along an incremental loading path. Jumps from one solution branch to other seem to be quite frequent.

In summary, although solutions of engineering utility can often be recovered by using the sort of steady state frictional description described in this work, there is significant evidence that stable, well-posed solutions in the steady state framework can be elusive for many parameter combinations. Although one can argue physically that certain parameter sets may be inconsistent with steady state solutions (particularly with respect to ω and v_g), it remains unclear whether the difficulties identified in this study are associated with the physical problem itself, the numerical discretization, or both.

Acknowledgements

This work was supported through a research contract by Michelin America Research Corporation. This support as well as collaboration of Mr. John Melson, Dr. Vasanti Gharpuray, Dr. Jean-Marc d'Harcourt, and Dr. Ali Rezgui is greatly appreciated.

Appendix A. Iterative Maps

A *positive orbit of the map, starting at point* $\boldsymbol{x}^0$ *is the sequence of images of that point under successive compositions of the map*, $\gamma^+(\boldsymbol{x}^0) = \{\boldsymbol{x}^0, \boldsymbol{g}(\boldsymbol{x}^0), \ldots, \boldsymbol{g}^i(\boldsymbol{x}^0), \ldots\}$.

A point $\bar{\boldsymbol{x}}$ is called a *fixed point of the map* if $\bar{\boldsymbol{x}} = \boldsymbol{g}(\bar{\boldsymbol{x}})$.

A point $\boldsymbol{x}^*$ is called a *periodic point of minimal period N* if $\boldsymbol{x}^* = \boldsymbol{g}^N(\boldsymbol{x}^*)$ and N is the smallest integer having this property. The set of iterates of such a point is called a *periodic orbit* or N-periodic solution of (2.1). By this definition, an equilibrium state of (2.1) is a period one solution (Guttalu, 1996).

Like fixed points, a N-periodic point can be stable, neutral or unstable according to whether or not the spectral radius of the N-fold composite of the map is less, equal or greater than one (for further reference see Kim and Feldstein, 1997).

A point $\boldsymbol{y}$ is called an *ω limit point* of the positive orbit $\gamma^+(\boldsymbol{x}^0)$ if there is a sequence of integers, n_i such that the subsequence $\boldsymbol{g}^{n_i}(\boldsymbol{x}^0)$ converges to it, i.e. there exists

$$\lim_{i\to\infty} \boldsymbol{g}^{n_i}(\boldsymbol{x}^0) = \boldsymbol{y}$$

The *linearization of the map at the fixed point*, $\boldsymbol{x} \to D\boldsymbol{g}(\bar{\boldsymbol{x}})\boldsymbol{x}$ where $D\boldsymbol{g}(\bar{\boldsymbol{x}})$ is the Jacobian matrix:

$$D\boldsymbol{g}(\bar{\boldsymbol{x}}) = \begin{pmatrix} \dfrac{\partial g_1}{\partial x_1}(\bar{\boldsymbol{x}}) & \cdots & \dfrac{\partial g_1}{\partial x_n}(\bar{\boldsymbol{x}}) \\ \cdots & \cdots & \cdots \\ \dfrac{\partial g_n}{\partial x_1}(\bar{\boldsymbol{x}}) & \cdots & \dfrac{\partial g_n}{\partial x_n}(\bar{\boldsymbol{x}}) \end{pmatrix} \tag{A.1}$$

The Jordan normal form of an $n \times n$ matrix is:

$$A_J = P^{-1}AP = \begin{pmatrix} \lambda_1 & 0 & 0 & 0 & 0 & 0 & 0 & 0 & 0 & 0 \\ 0 & \ddots & 0 & 0 & 0 & 0 & 0 & 0 & 0 & 0 \\ 0 & 0 & \lambda_k & 0 & 0 & 0 & 0 & 0 & 0 & 0 \\ 0 & 0 & 0 & \ddots & 0 & 0 & 0 & 0 & 0 & 0 \\ 0 & 0 & 0 & 0 & \lambda_m & 1 & 0 & 0 & 0 & 0 \\ 0 & 0 & 0 & 0 & 0 & \ddots & 1 & 0 & 0 & 0 \\ 0 & 0 & 0 & 0 & 0 & 0 & \lambda_m & 0 & 0 & 0 \\ 0 & 0 & 0 & 0 & 0 & 0 & 0 & \ddots & 0 & 0 \\ 0 & 0 & 0 & 0 & 0 & 0 & 0 & 0 & \alpha & -\beta \\ 0 & 0 & 0 & 0 & 0 & 0 & 0 & 0 & \beta & \alpha \end{pmatrix} \tag{A.2}$$

where the entries of the form: $\begin{pmatrix} \lambda_m & 1 & 0 \\ 0 & \ddots & 1 \\ 0 & 0 & \lambda_m \end{pmatrix}$ are called Jordan blocks.

The stability of a fixed point can sometimes be characterized by studying the linearization of the map. A fixed point $\bar{\boldsymbol{x}}$ is said to be *hyperbolic* if the Jacobian matrix at $\bar{\boldsymbol{x}}$ has no eigenvalues of modulus one. The stability of such point is easy to determine. If all eigenvalues have moduli less than one, then the point is asymptotically stable while one eigenvalue with modulus greater than one implies instability.

Through an elementary linear transformation (with a nonsingular transformation matrix), any $n \times n$ matrix can be put in the Jordan normal form having on the diagonal:

1. The eigenvalues (if these are simple or multiple but with equal geometric and algebraic multiplicity;
2. Jordan blocks for corresponding to multiple eigenvalues with different geometric and algebraic multiplicity;

3. 2×2 blocks of the form: $\begin{pmatrix} \alpha & -\beta \\ \beta & \alpha \end{pmatrix}$ corresponding to complex conjugate pairs of eigenvalues.

In this section we are only interested in the occurrence of blocks of the last type in the linearized map that can also be written in the alternate form: $A = \lambda \begin{pmatrix} \cos\theta & -\sin\theta \\ \sin\theta & \cos\theta \end{pmatrix}$ where $\lambda = \sqrt{(a^2 + b^2)}$. The action of map A is in this case to rotate the vector with an angle θ and scale it with the factor λ. Nonhyperbolic points (corresponding to λ=1) have a more complex stability behavior. The linear map undergoes a bifurcation at such points in the sense that for $\lambda \neq 1$ closed orbits invariant under the map do not exist but for $\lambda = 1$ there is a closed invariant orbit. Such an orbit in the case of the linear map lies on the circle and it is periodic if $\frac{\theta}{2\pi} \in \mathbf{Q}$ and dense if $\frac{\theta}{2\pi}$ is irrational.

It is obvious that if $\bar{\boldsymbol{x}}$ is a k-periodic point, so are $\boldsymbol{g}^i(\bar{\boldsymbol{x}})$ for all $i = \bar{1}, \ldots, k-1$ and an orbit of the map starting at $\bar{\boldsymbol{x}}$ is a k-cycle. Stability of all k-periodic points implies stability of the k-cycle. An iterative map often exhibits such stable k-cycles.

In the nonlinear case, the equivalent is called an *Andronov–Hopf bifurcation*. When the eigenvalues move across the unit circle, there appears a closed invariant curve (orbits starting on any point on this curve remain on the curve) which encloses the fixed point. Therefore if a current iterate happens to fall on one of this curves, convergence will not be obtained through the Newton–Raphson algorithm.

The simplest nonlinear map illustrating the birth of an invariant closed orbit (local bifurcation near a fixed point) is the nonlinear planar map:

$$\begin{pmatrix} r \\ \theta \end{pmatrix} \to \begin{pmatrix} \lambda r - r^3 \\ \theta + \omega \end{pmatrix} \tag{A.3}$$

whose linearization falls under the form of the blocks of the third type.

For $\lambda > 1$ the map has an invariant circle of radius $r = \sqrt{\lambda - 1}$ and the iterates of the map are rotations of angle ω. When λ passes 1, the asymptotically stable fixed point becomes unstable and an invariant stable circle appears.

A more general result is proven in the Poincaré–Andronov–Hopf theorem (see for reference Hale and Kocak, 1991) by transforming locally any nonlinear map into a "canonical" form similar to the example above.

References

Andersson, L.-E., Klarbring, A., 2002. Existence and uniqueness for quasistatic contact problem with friction. In: Martins, J.A.C., Monteiro Marques, M.D.P. (Eds.), Contact Mechanics. Springer, pp. 245–260.

Ballard, P., 1999. A counter example to uniqueness in quasi-static elastic contact problem with small friction. International Journal of Engineering Science.

Chatterjee, J.P., Cusumano, A., Zolock, J.D., 1999. On contact-induced standing waves in rotating tires: experiment and theory. Journal of Sound and Vibration 227 (5), 1049–1081.

Chau, O., Motreanu, D., Sofonea, M., 2002. Quasistatic frictional problems for elastic and viscoelastic materials. Applications of Mathematics 47 (4), 341–360.

Doudoumis, I., Mitsopoulou, E., Charalambakis, N., 1994. The influence of the friction coefficients on the uniqueness of the solution of the unilateral contact problem. In: Raous, M., Jean, M., Moreau, J.J. (Eds.), Contact Mechanics. Plenum Press, pp. 79–86.

Guttalu, R.S., 1996. On an improved simple cell mapping unravelling algorithm. Nonlinear Dynamics and Controls, ASME 91, 27–32.

Hassani, R., Hild, P., Ionescu, I.R., 2004. Sufficient conditions of non-uniqueness for the coulomb friction problem. Mathematical Methods in the Applied Sciences 27, 47–67.

Hassani, R., Hild, P., Ionescu, I.R., Sakki, N.-D., 2003. A mixed finite element method and solution multiplicity for coulomb frictional contact. Computer Methods in Applied Mechanics and Engineering 192, 4517–4531.

Hale, J., Kocak, H., 1991. Dynamics and Bifurcations. Springer-Verlag.

Han, W., Schillor, M., Sofonea, M., 2001. Variational and numerical analysis of a quasistatic viscoelastic problem with normal compliance friction, and damage. Journal of Computational and Applied Mathematics 132, 377–398.

Han, W., Sofonea, M., 2002. Quasistatic Contact Problems in Viscoelasticity and Viscoplasticity Studies in Advanced Mathematics, vol. 30, American Mathematical Society, International Press.

Kim, Y.I., Feldstein, A., 1997. Bifurcation and k-cycles of a finite dimensional iterative map with application to logistic delay equations. Applied Numerical Mathematics 24, 411–424.

Kouhia, R., Mikkola, M., 1998. Numerical treatment of multiple bifurcation points. In: Computational Mechanics, New Trends and Applications, Proceedings of the Fourth World Congress of Computational Mechanics, Buenos Aires, Argentina, June 29–July 2.

Laursen, T.A., 2002. Computational Contact and Impact Mechanics. Springer.

Laursen, T.A., Stanciulescu, I., 2005. An algorithm for incorporation of frictional sliding conditions within a steady state rolling framework. In: Communications in Numerical Methods in Engineering, in press.

Le Tallec, P., Rahier, C., 1994. Numerical models of steady rolling for non-linear viscoelastic structures in finite deformations. International Journal of Numerical Methods in Engineering 37, 1159–1186.

Narayanan, S., Sekar, P., 1996. Bifurcation and chaos in parametrically excited contact vibrations. Nonlinear Dynamics and Controls ASME 91, 59–65.

Oden, J.T., Lin, T.L., 1986. On the general rolling contact problem for finite deformations of a viscoelastic cylinder. Computer Methods in Applied Mechanics and Engineering 57, 297–367.

Oden, J.T., Rabier, P.J., 1989. Bifurcation in Rotating Bodies, MASSON & Springer-Verlag.

Planinc, I., Saje, M., 1999. A quadratically convergent algorithm for the computation of stability points: the application of the determinant of the tangent stiffness matrix. Computer Methods in Applied Mechanics and Engineering 169, 89–105.

Riks, E., 1972. The application of newton's method to the problem of elastic stability. Journal of Applied Mechanics, 1060–1065.

Simo, J.C., Taylor, R.L., Wriggers, P., 1991. A note of finite element implementation of pressure boundary loading. Communications in Applied Numerical Methods 7 (7), 513–525.

Taylor, R.L., 2003. A Finite Element Analysis Program, Version 7.5.

Wriggers, P., 2002. Computational Contact Mechanics. John Wiley & Sons Ltd.

Wriggers, P., Simo, J.C., 1990. General procedure for the direct computation of turning and bifurcation points. International Journal of Numerical Methods in Engineering 30, 155–176.

Wriggers, P., Wagner, W., Miehe, C., 1988. Quadratic convergent procedure for the calculation of stability points in finite element analysis. Computer Methods in Applied Mechanics and Engineering 70, 329–347.